symmetry

MDPI

Article

A Hybrid Swarming Algorithm for Adaptive Enhancement of Low-Illumination Images

Yi Zhang [1,2], Xinyu Liu [1] and Yang Lv [1,*]

[1] College of Electrical and Computer Science, Jilin Jianzhu University, 5088 Xincheng Street, Changchun 130118, China; zhangyi@jlju.edu.cn (Y.Z.); lxinyu105@hotmail.com (X.L.)
[2] Key Laboratory for Comprehensive Energy Saving of Cold Regions Architecture of Ministry of Education, Jilin Jianzhu University, 5088 Xincheng Street, Changchun 130118, China
* Correspondence: lvyang4737@hotmail.com

Abstract: This paper presents an improved swarming algorithm that enhances low-illumination images. The algorithm combines a hybrid Harris Eagle algorithm with double gamma (IHHO-BIGA) and incomplete beta (IHHO-NBeta) functions. This paper integrates the concept of symmetry into the improvement steps of the image adaptive enhancement algorithm. The enhanced algorithm integrates chaotic mapping for population initialization, a nonlinear formula for prey energy calculation, spiral motion from the black widow algorithm for global search enhancement, a nonlinear inertia weight factor inspired by particle swarm optimization, and a modified Levy flight strategy to prevent premature convergence to local optima. This paper compares the algorithm's performance with other swarm intelligence algorithms using commonly used test functions. The algorithm's performance is compared against several emerging swarm intelligence algorithms using commonly used test functions, with results demonstrating its superior performance. The improved Harris Eagle algorithm is then applied for image adaptive enhancement, and its effectiveness is evaluated on five low-illumination images from the LOL dataset. The proposed method is compared to three common image enhancement techniques and the IHHO-BIGA and IHHO-NBeta methods. The experimental results reveal that the proposed approach achieves optimal visual perception and enhanced image evaluation metrics, outperforming the existing techniques. Notably, the standard deviation data of the first image show that the IHHO-NBeta method enhances the image by 8.26%, 120.91%, 126.85%, and 164.02% compared with IHHO-BIGA, the single-scale Retinex enhancement method, the homomorphic filtering method, and the limited contrast adaptive histogram equalization method, respectively. The processing time of the improved method is also better than the previous heuristic algorithm.

Keywords: low-illumination image; Harris Eagle algorithm; histogram equalization; gamma correction function; incomplete beta function

Citation: Zhang, Y.; Liu, X.; Lv, Y. A Hybrid Swarming Algorithm for Adaptive Enhancement of Low-Illumination Images. *Symmetry* **2024**, *16*, 533. https://doi.org/10.3390/sym16050533

Academic Editor: Aviv Gibali

Received: 28 February 2024
Revised: 29 March 2024
Accepted: 17 April 2024
Published: 29 April 2024

1. Introduction

Various factors often affect low-light images, such as imperfections in imaging systems, recording devices, and transmission media. Incomplete processing methods can lead to decreased image quality because the output signal level of the imaging system falls below a specified value of the scene brightness. Such images exhibit low brightness, weakened detail information, poor contrast, color distortion, a narrow grayscale range, and high interference, significantly impacting human visual perception and the efficiency of machine vision-related systems. Specific application scenarios, such as underwater images, are influenced by water's absorption and scattering of light [1], resulting in color shifts and reduced contrast. Foggy weather images are affected by fog's refraction and light obstruction [2], leading to low brightness and poor clarity. Medical images are impacted by noise interference, poor lighting, and other factors [3], resulting in missing detailed information and high noise levels. These challenges hinder human productivity and daily life. Image enhancement technology is a crucial component of the image processing process. Its primary objective is to process image information effectively, enhance the appearance of low-quality images, and ultimately improve visual effects while minimizing noise amplification and maintaining good real-time performance. Image enhancement not only effectively improves human subjective visual perception but also enhances the efficiency, reliability, and robustness of visual systems.

Low-illumination image enhancement research has rapidly gained traction as a research hotspot because of its wide range of applications, resulting in numerous emerging research outcomes. Each image enhancement technique has its own set of advantages and disadvantages. Prevalent image enhancement methods include spatial domain, frequency domain, image fusion, Retinex, and deep learning. Spatial methods encompass techniques such as the histogram equalization algorithm [4], the gamma correction algorithm [5], the beta correction algorithm [6], and median filter [7]. Frequency domain methods comprise low-pass filters [8], homomorphic filters [9], and high-pass filters [10]. Image fusion methods include exposure interpolation [11] and multi-image fusion [12]. The classic methods for image enhancement based on Retinex's theory include the single-scale algorithm (SSR) [13], the multi-scale algorithm (MSR) [14], and the algorithm with color restoration (MSRR) [15]. Deep learning-based methods primarily involve techniques based on convolutional neural networks (CNNs) [16], adversarial genetic networks (GANs) [17], and methods that combine deep learning with Retinex theory [18]. Swarm intelligence algorithms are known for their excellent convergence performance and optimization abilities, making them widely applicable in various fields including image enhancement. Numerous new algorithms are being developed as swarm intelligence algorithms continue to evolve. Furthermore, traditional swarm intelligence algorithms, such as [19–21], are being optimized and improved. Emerging algorithms have also found applications in image enhancement because of their outstanding performance, such as the marine predator algorithm (MPA) [22] and the salp swarm optimization algorithm (SSOA) [23].

This paper proposes an adaptive low-illumination image enhancement method based on an improved Harris Hawk algorithm. The image is adaptively enhanced by combining two correction functions with an improved algorithm by using the concept of symmetry. This improved method combines gamma correction and incomplete beta functions to enhance images in low-illumination conditions. This combination effectively addresses the challenges of low brightness, poor contrast, weak detail information, and noise in low-illumination images. The processing time of the proposed method is improved to some extent compared with the other strategies. The contributions of this article can be summarized as follows:

- **Improved Harris Hawk Algorithm.** Firstly, this paper proposes employing circle chaotic mapping for population initialization to solve the issues of slow convergence and susceptibility to local optimality in the Harris Hawk algorithm. This improvement enhances the search capabilities of the Harris Hawk and enriches population information. This paper also replaces the original energy conversion formula with a nonlinear dynamic formula to expedite transitions between global and local searches, significantly improving convergence speed. Additionally, this work incorporates the spiral motion from the black widow algorithm to improve global search behavior and strengthen the Harris Eagle algorithm's ability to escape local optima. A nonlinear inertia weight factor from the particle swarm optimization algorithm is introduced to accelerate the local search speed. Finally, this work corrects some issues in the original algorithm's Levy flight.
- **Adaptive Enhancement of Low-Illuminance Images.** This study employs a swarm intelligence algorithm and a correction function to enhance low-illuminance images. The entropy of an image is a statistical form of features that reflects the average amount of information in the image and represents the clustering characteristics of the grayscale distribution of the image, so we use image entropy as a fitness function to optimize the parameters of the gamma correction function and incomplete beta function, enabling us

to identify the optimal parameter values and achieve the best low-illuminance image enhancement results.

• **Comparison with other methods through experiments.** This study enhances five low-illumination images from the LOL [24] dataset. The comparison experiment includes limited contrast adaptive histogram equalization (CLAHE), single-scale Retinex enhancement (SSR), homomorphic filtering, and the method proposed in this paper. After enhancement, the average gradient (AG), standard deviation (SD), spatial frequency (SF), information entropy (IE), and correlation coefficient (CC) serve as evaluation indices. The entropy of the five images enhanced by IHHO-Nbeta increases by 76.84%, 59.01%, 71.47%, 51.03%, and 44.02%, respectively, compared with the original low-illumination images. For example, considering the enhancement effect on the first image, the standard deviation of IHHO-NBeta increases by 8.26% compared with IHHO-BIGA and 120.91% compared with SSR.

This paper is organized into five sections. The first section serves as an introduction, primarily discussing the background of low-illumination image enhancement. The second section on related works presents an overview of the current research progress in this area. The third section focuses on the methodology, which involves the improvement in the Harris Eagle algorithm, using the enhanced Harris Eagle in conjunction with the double gamma correction function and incomplete beta function for adaptive image enhancement. The fourth section details the experiments conducted in this study. Seven standard test functions are employed to compare the improved algorithms, encompassing a variety of emerging swarm intelligence algorithms. Additionally, the proposed method is compared with several other image enhancement techniques, demonstrating the superior performance of the method proposed in this study. Finally, a quantitative comparison is made on the processing time of image enhancement. The fifth and final section summarizes the entirety of this study and outlines prospects for future research.

2. Related Works

Numerous image enhancement methods have been optimized in recent years. Each has unique advantages and disadvantages. Histogram equalization optimization is a well-established image enhancement technique that increases contrast and detail content by extending the range of gray values. A novel three-part histogram equalization method is proposed in the literature [25]. The improvements can effectively enhance images by dividing them into three sub-regions and performing histogram equalization processing. However, the abnormal stretching of gray levels can result in artifacts, sawtooth effects, and over-enhancement when histogram equalization is applied for image enhancement. Various solutions have been proposed by researchers to address these issues. Majid et al. [26] introduced a triple-clipping dynamic histogram equalization optimization algorithm, but the performance of this method has room for improvement. Bhupendra et al. [27] effectively overcame the mean shift problem and enhanced contrast by dividing the quantiles of the histogram.

The Contrast Limited Adaptive Histogram Equalization (CLAHE) is a development based on the histogram equalization method. The primary distinction between CLAHE and its predecessors is contrast limiting. CLAHE effectively avoids the issue of excessive noise amplification caused by histogram equalization. In a study by [28], CLAHE enhanced retinal fundus images, yielding outstanding results. Lu et al. [29] employed CLAHE, the Gauss mask algorithm, and differential processing to enhance weld images. This approach effectively removed noise and retained edge information while improving contrast.

Gamma and incomplete beta correction offer simplicity and convenience but can result in over-enhancement, under-enhancement, and color distortion when enhancing low-illumination images. Jeon et al. [30] demonstrated that a cross-correlation color histogram translation algorithm combined with gamma correction could effectively resolve red artifacts in dust images and reduce color distortion. Lee et al. [31] proposed a blind inverse gamma correction algorithm suitable for multiple types of image enhancement.

Liu et al. [32] developed a simple and efficient method based on membership function and gamma correction, which can overcome over- and under-enhancement issues during image enhancement.

In addition to the optimizations for histogram equalization and gamma correction, some studies have combined the two methods. For example, [33] used particle swarm optimization to optimize the histogram equalization of gamma correction, effectively avoiding excessive enhancement and unnatural artifacts. Inspired by this research, an increasing number of swarm intelligence algorithms are being applied to image enhancement, such as FPA [34] and the Selfish Herd Optimizer (SHO) [35]. Yan et al. [36] enhanced images of autonomous underwater vehicles using the whale algorithm. Liu et al. [37] effectively avoided image color distortion and excessive noise by using the parameters of the multi-objective Grasshopper algorithm (GOA), the Duffing oscillator model, and the homomorphic filter. Sun et al. [38] fused images optimized by the artificial bee colony algorithm with weights and compared the results with histogram equalization and double gamma correction, proving that the proposed algorithm can emphasize details and reduce noise. The related works are summarized in Table 1.

Table 1. The benefits and shortcomings of related works.

Related Works	Methods	Benefits and Shortcomings
[25]	three-part histogram equalization	effectively enhanced images; artifacts, sawtooth effects, and over-enhancement
[26]	triple-clipping dynamic histogram equalization	the performance has room for improvement
[27]	divided the quantiles of the histogram	overcame the mean shift problem and enhanced contrast; excessive noise amplification
[28]	enhanced retinal fundus images	avoided excessive noise amplification; results may not be ideal for details
[29]	CLAHE, Gauss mask algorithm, and differential processing	removed noise and retained edge information while improving contrast; the noise point of the weld image has not been effectively improved
[30]	a cross-correlation color histogram translation algorithm	resolved red artifacts in dust images and reduced color distortion
[31]	a blind inverse gamma correction algorithm	can be seamlessly extended to a masked image and multi-channel image, and is free of the arbitrary tuning parameter
[32]	a simple and efficient method based on the membership function and gamma correction	overcame over- and under-enhancement issues
[33]	used particle swarm optimization to optimize the histogram equalization of gamma correction	avoided excessive enhancement and unnatural artifacts
[34]	used FPA to optimize the histogram equalization of gamma correction	produceed more robust, scalable, and precise results than the original FPA
[35]	used SHO to optimize the histogram equalization of gamma correction	two different solutions
[36]	used the whale algorithm	enhanced images of autonomous underwater vehicles
[37]	used the parameters of the multi-objective Grasshopper algorithm (GOA), the Duffing oscillator model, and thhe homomorphic filter	effectively avoided image color distortion and excessive noise
[38]	the artificial bee colony algorithm with weights	emphasized details and reduced noise

Based on this investigation and summary of the existing methods, it is not difficult to find that there are certain shortcomings in the current methods applied to image enhancement. As more and more swarm intelligence methods are applied in image enhancement, finding ways to improve the performance of algorithms is becoming increasingly important. The method proposed in this article is experimentally compared and shows improvements in both processing time and performance compared with other classic traditional methods.

3. Methods

3.1. Traditional Image Enhancement Methods

There are many traditional image enhancement methods, most of which require less time processing, but the enhancement effect is average. The difference between CLAHE and ordinary adaptive histogram equalization lies in contrast limiting, which is often used to overcome the excessive amplification of noise by AHE. Compared with AHE, CLAHE has two improvements as follows: a proposed histogram distribution method and an interpolation method. In the histogram distribution method, there is a threshold to crop a certain grayscale value in the histogram that exceeds the threshold, and then evenly distributes the parts that exceed the threshold to each grayscale level. The proposed interpolation method divides the image into blocks, which can effectively avoid the defects of discontinuous blocks. The flowchart is shown in Figure 1.

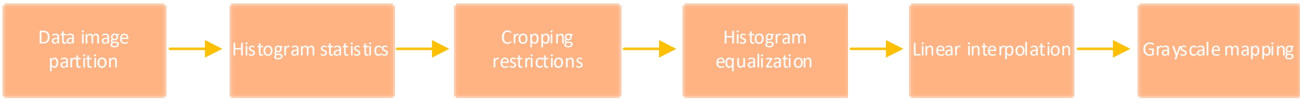

Figure 1. Flowchart for CLAHE.

Retinex is a commonly used image enhancement method whose theoretical basis is that the color of an object is determined by the reflection ability of the object to different wavelengths of light, and the color of the object is not affected by light non-uniformity, with consistency. Retinex can achieve a balance between dynamic compression, edge enhancement, and color constancy, thus enabling adaptive enhancement of various types of images. SSR is one of the earliest image enhancement methods based on Retinex, and its flowchart is shown in Figure 2.

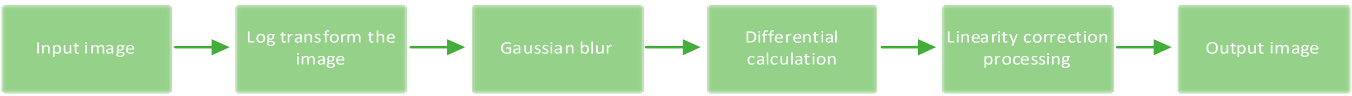

Figure 2. Flowchart for SSR.

Homomorphic filtering is a method of enhancing an image using the frequency domain. It reduces the impact of light changes on the image by reducing the low-frequency portion and enhancing the high-frequency portion through filtering algorithms. This method can handle the problems of a large dynamic range, uneven image illumination, and unclear details in dark areas in images. Based on the nonlinear characteristics of the human eye's response to brightness, this method not only enhances image details in dark areas but also does not lose image details in bright areas, thus achieving the effect of image enhancement. The flowchart is shown in Figure 3.

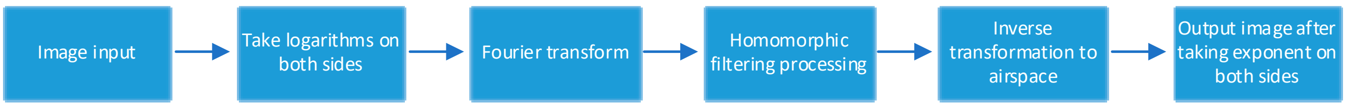

Figure 3. Flowchart for homomorphic filtering.

3.2. Improved Harris Hawk Algorithm

At present, some researchers are attempting to improve the accuracy and convergence of the algorithm results by increasing the time complexity of the operation, but sacrificing time complexity will bring great challenges to computational resources and solving time. The improved operations in this paper are derived without changing the time complexity of the original heuristic algorithm. The Harris Hawk algorithm (HHO) is a new type of swarm intelligence algorithm proposed in 2019 [39]. It mainly searches for the optimal solution by simulating the predatory behavior of the Harris Hawk. HHO is an excellent heuristic algorithm. It does not have many parameters to adjust and has good performance. Compared with other heuristic algorithms, HHO has good search performance and the ability to jump out of local optima. HHO mainly includes the following three key steps: global search, conversion stage, and local search. The global search involves dividing two searches' formulas into equal probabilities using a random number as follows:

$$X(t+1) = \begin{cases} X_{rand}(t) - r_1|X_{rand}(t) - 2r_2X(t)|q \geq 0.5 \\ (X_{rabbit}(t) - X_m(t)) - r_3(lb + r_4(ub - lb))q < 0.5 \end{cases}$$

$$X_m(t) = \frac{1}{N}\sum\nolimits_{i=1}^{N} X_i(t) \tag{1}$$

In Formula (1), $X(t)$ represents the current position, $X_{rand}(t)$ represents a random position, $X_{rabbit}(t)$ and $X_m(t)$ represent the prey's position and average position, respectively, r represents a random number, q represents the strategy selection probability, and N represents the population number. The transformation stage is represented by a simple linear formula, i.e., Formula (7), which includes four strategies of a Harris Hawk in the local search, as shown in the Table 2:

Table 2. Four local search strategies of the Harris Hawk condition formula.

Strategy	Condition	Formula	
Soft surround	$r \geq 0.5, 1 > \lvert E\rvert \geq 0.5$	$X(t+1) = \Delta X(t) - E\lvert JX_{rabbit}(t) - X(t)\rvert$ $\Delta X(t) = X_{rabbit}(t) - X(t)$ $J = 2(1 - r_5)$	(2)
Hard surround	$r \geq 0.5, 0.5 > \lvert E\rvert$	$X(t+1) = X_{rabbit}(t) - E\lvert\Delta X(t)\rvert$	(3)
Quick glide Soft surround	$r < 0.5, 1 > \lvert E\rvert \geq 0.5$	$X(t+1) = \begin{cases} YF(Y) < F(X(t)) \\ ZF(Z) < F(X(t)) \end{cases}$ $Z = Y + S \times LF(D)$ $Y = X_{rabbit}(t) - E\lvert JX_{rabbit}(t) - X(t)\rvert$	(4)
Quick glide hard surround	$r < 0.5, 0.5 > \lvert E\rvert$	$X(t+1) = \begin{cases} YF(Y) < F(X(t)) \\ ZF(Z) < F(X(t)) \end{cases}$ $Z = Y + S \times LF(D)$ $Y = X_{rabbit}(t) - E\lvert JX_{rabbit}(t) - X_m(t)\rvert$	(5)

Detailed explanations of Formulas (1)–(5) in the above table can be found in the literature [39]. In the above equation, r represents a random number, E represents the energy formula, $\Delta X(t)$ represents the position difference in the Harris Hawk, J represents ta random number between 0 and 2, Z simulates the glide process, and Y simulates the movement process of the approach. Aiming at the characteristics of HHO such as low population richness, easily falling into local optimization, and slow convergence speed, this study made improvements to several parts of the Harris Hawk algorithm. The improvement methods are all carried out without changing the time complexity of the algorithm itself, including improvements to initialization and search strategies.

Many meta-heuristic algorithms use a random strategy when initializing populations, significantly reducing the richness of simulated biological populations. Many studies use chaotic mapping to map variables into the value range of the chaotic variable space and linearly transform the problem's solution into the optimal variable space to solve this problem, such as [40]. In this study, chaotic mapping is introduced into the initial population stage of the Harris Hawk algorithm, and a circle map is used to initialize the population. The improved initial position distribution of the population is more uniform compared with the random initialization. This part of the disturbance to population chaos reflects the idea of symmetry. This method not only broadens the search space of the Harris Hawk and increases the diversity of group location but also avoids the local optimization of the algorithm to a certain extent and improves the algorithm's efficiency. The circle mapping formula, i.e., Formula (6), is as follows:

$$x_{i+1} = mod\left(x_i + 0.2 - \left(\frac{0.5}{2\pi}\right) sin(2\pi x_i), 1\right) \quad (6)$$

where x_i in Formula (6) represents an individual position and *mod* represents modular operation.

The convergence speed of the Harris Hawk algorithm is largely influenced by the energy conversion formula. In the original text of the Harris Hawk algorithm, the author adopted a linear formula to simulate the process of decreasing prey energy with an increase in iteration times. However, the dynamic process of prey energy changes is not reflected by using the linear formula in the original text. That is, in the early stages of encirclement, the prey's energy is high and vigorous; during the process of encirclement, the prey constantly moves to avoid the Harris Eagle, and energy is rapidly consumed; and at the end of the iteration, the prey is already exhausted, and its energy will remain at a low level and continue to decline. To optimize this process, this study uses a nonlinear dynamic formula instead of the original formula:

$$E = 2 * (1 - (\frac{t}{T})) \quad (7)$$

$$E = \beta_1 * exp(-30 * (\frac{t}{T})^{\alpha_1}) \quad (8)$$

In Formulas (7) and (8), t represents the current number of iterations, T represents the maximum number of iterations, β_1 represents the amplitude coefficient, and α_1 is an exponential parameter. The improved energy formula can be more appropriate to the energy process of the prey, as shown in Figure 4, and the energy remains at a high level at the beginning of the iteration. Figure 5 above shows that the exponential parameters are taken as 3, 5, and 10, respectively. In the middle of the iteration, the prey's energy will rapidly decline; at the end of the iteration, the prey's energy remains at a low level and continues to decline. The algorithm can dynamically search at different search stages through this improved energy formula. The energy formula is an important factor connecting different search strategies in the design of the algorithm, and this nonlinear dynamic search can improve the efficiency of the algorithm.

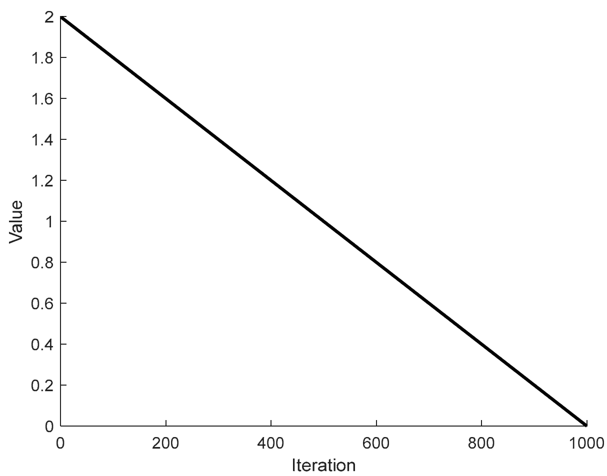

Figure 4. Linear energy formula in the original algorithm.

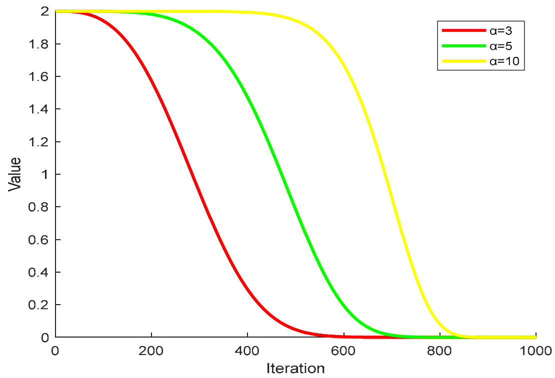

Figure 5. The nonlinear dynamic formula proposed in this study.

The Harris Hawk algorithm has the disadvantage of easily falling into local optimization during the iterative process. Many scholars have conducted many studies to solve the above problems, such as [41]. The linear motion and spiral motion in the black widow algorithm adopt the guidance mechanism of the optimal individual, which is a key step in the black widow algorithm to reduce the population falling into a local optimal. The original author continued the idea of the black widow algorithm and proposed a jumping spider algorithm in the design of subsequent algorithms. The missing spiral search strategy makes it perform mediocrely in the global search process, although it performs outstandingly in continuous unimodal functions. This study introduced the spiral motion behavior of spiders in the black widow algorithm [42] into the global search to strengthen the ability of the Harris Eagle algorithm to jump out of local optima, and the improvement also be used to characterize the circling behavior of Harris Hawks during the global search.

$$\vec{x}_i(t+1) = \begin{cases} \vec{x}_*(t) - m\vec{x}_{r1}(t), if\ rand() \leq 0.3 \\ \vec{x}_*(t) - cos(2\pi\beta_2)\vec{x}_i(t), in\ other\ case \end{cases} \tag{9}$$

The improved Harris Eagle global search process is:

$$x(t+1) = \begin{cases} x_{rand}(t) - |x_{rand}(t) - cos(2\pi\beta_2)x(t)|, q \geq 0.5 \\ [x_{rabbit}(t) - x_m(t)] - r[lb + r(ub - lb)], q < 0.5 \end{cases} \tag{10}$$

In Formula (9) above, m is a random number in [0.4, 0.9], β_2 is a random number in [−1, 1], and $\vec{x}_*(t)$ indicates the optimal location for the black widow spider. $x_{rand}(t)$ in (10) represents the random position of the Harris Eagle, $x_{rabbit}(t)$ represents the prey's position, and $x_m(t)$ represents the average position. lb, ub, and r represent the lower limit positions, upper limit positions, and random numbers, respectively. q is used to represent the transition of the Harris Hawk search strategy with equal probability.

Many studies have optimized the local search stage of the Harris Hawk to accelerate the convergence speed of the Harris Hawk algorithm. Zhang et al. [43] introduced the sine and cosine algorithm into the Harris Hawk algorithm, using the oscillating optimization process of the sine and cosine to accelerate the convergence speed of the Harris Hawk. This paper adds a nonlinear inertia weight factor to the local search process of the Harris Hawk algorithm, which originates from the acceleration of the particle swarm algorithm by the inertia weight factor in the inertia weight particle swarm algorithm. The nonlinear inertia weight factor can make the convergence speed of the algorithm change with the number of iterations. At the beginning of the iteration, the inertia factor is small, and as the number of iterations increases, the value of the nonlinear inertia factor gradually increases first and then decreases. The nonlinear inertia factor formula is as follows:

$$w\_now = \left(sin(\pi * \frac{t}{T}) * (w\_start - w\_end) \right) + w\_end \quad (11)$$

In Equation (11), w_start and w_end represent the initial inertia weight and the end inertia weight, respectively. The value changes with the number of iterations, as shown in Figure 6.

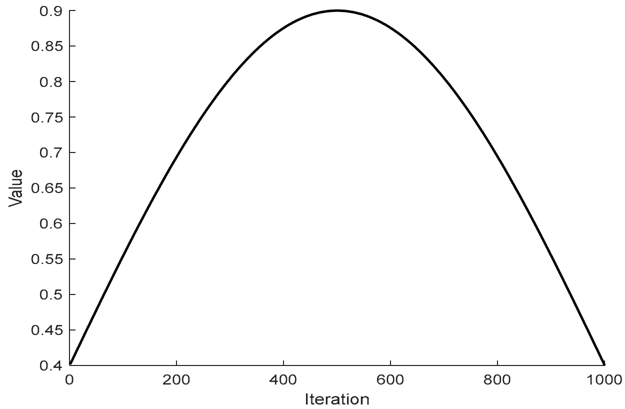

Figure 6. Inertia weight factor curve.

The nonlinear inertia weighting factor can be combined with the improvement in the Harris Hawk algorithm using the nonlinear dynamic energy formula mentioned above. When the prey's energy decreases rapidly in the middle of the iteration, the inertia weight factor also remains at a high level, which can accelerate the conversion of the algorithm from a global search to a local search and enable the Harris Hawk algorithm to conduct a local search at a faster speed.

The Levy flight strategy is often used in swarm intelligence algorithms based on birds or swimming fungi [44,45] to simulate the gliding behavior of organisms. Levy flight has the characteristics of alternating long and short lengths, strong randomness, and the ability to jump out of local optima, which is relatively consistent with heuristic algorithms. In the Harris Hawk algorithm, the author also uses Levy flight to simulate the gliding process of a Harris Hawk during predation. However, the Levy flight formula in the original text has certain defects. The Levy formula in the original text is as follows:

$$LF(x) = \alpha_3 \times \frac{u \times \sigma}{|v|^{\frac{1}{\beta_3}}} \qquad \sigma = \left(\frac{\Gamma(1+\beta_3) \times sin(\frac{\pi\beta_3}{2})}{\Gamma\left(\frac{1+\beta_3}{2}\right) \times \beta_3 \times 2^{(\frac{\beta_3 - 1}{2})}} \right)^{\frac{1}{\beta_3}} \quad (12)$$

Formula (12) above conforms to the Markov construction process. In the formula, α_3 is a characteristic coefficient, and it takes a value of 0.01 in the original text. The value range of parameter β_3 is generally between 0 and 2, and in the original text, it takes a value of 1.5. In the original algorithm, u and v are represented by random numbers between [0,1]. This paper uses the positive distribution in the Mantegna method to process u and v in Formula (12) to correct this. The pseudocode of the improved Harris Eagle algorithm is as follows in Algorithm 1:

The computational complexity of the IHHO mainly depends on the following three processes: initialization of added disturbances, fitness evaluation, and population position update. Assuming the population size is N, the computational complexity of the initialization part is O (D × N). The computational complexity of evaluating the optimal location and updating the population position vector is O (N × T + N × T × D). In summary, the computational complexity of the IHHO is O (N × (T + D + T × D)).

Algorithm 1. Improved Harris Hawk algorithm

Require: Initialize related parameters
Ensure: Initialize population using circle chaotic map 6
Ensure: Optimize prey energy E through Formula (8)
while $t < T_0$ **do**
    if abs(E) ≥ 1 **then**
        Perform global search according to Formula (10)
    else abs(E) < 1 **then**
        if $r \geq 0.5$ and abs(E) > 0.5 **then**
            Use Formula (9) to improve soft surrounding
        end if
        if $r \geq 0.5$ and abs(E) < 0.5 **then**
            Use Formula (9) to improve hard surrounding
        end if
        if $r < 0.5$ and abs(E) > 0.5 **then**
            Fast gliding soft surrounding for Levy correction (12) and nonlinear inertia weight optimization
        end if
        if $r < 0.5$ and abs(E) < 0.5 **then**
            Fast gliding hard surround for Levy correction (12) and nonlinear inertia weight optimization
        end if
    end if
end while

3.3. Adaptive Enhancement of Low-Illuminance Images Based on the Improved Harris Hawk Algorithm and Gamma Correction

Gamma correction has a good effect on brightness correction. Its principle is to edit the gamma curve of an image, using a non-linear tone editing method to detect dark and light parts and increase the ratio of the two, thereby achieving the effect of image enhancement. The expression for gamma correction is:

$$f(I) = cI^{\gamma} \tag{13}$$

In Equation (13), I represent the grayscale value of the input image, and both c and γ represent correction coefficients. Different values will have different enhancement effects on the image. However, for images with different grayscale values and display effects, the effect of gamma correction is single, and some important information may be missing. Therefore, this paper introduces the BIGA method [46] to process images through two gamma functions, which can improve the intensity of dark light while suppressing the enhancement of bright areas and can avoid excessive enhancement of color images. The global dual gamma correction expression is as follows:

$$G_a(x) = x^{\frac{1}{\gamma}} \tag{14}$$

$$G_b(x) = 1 - \Big(1 - x\Big)^{\frac{1}{\gamma}} \tag{15}$$

$$G(x) = \alpha G_a(x) + (1 - \alpha) G_b(x) \tag{16}$$

$G_a(x)$ and $G_b(x)$ in Equations (14)–(16) are convex and concave functions, respectively, that are used to enhance dark regions and suppress bright regions. To enhance low-illumination images using the improved Harris Eagle algorithm, it is first necessary to normalize the image, use the global dual gamma correction formula to enhance the normalized gray level information, and then restore the enhanced information to the range of [0, 255] through the inverse normalization process. Using the improved Harris Eagle algorithm to optimize the enhanced image information α value enables enhanced images to obtain higher fitness values with the following pseudocode in Algorithm 2:

Algorithm 2. Low-illumination image enhancement based on the improved Harris Hawk algorithm and gamma correction

Require: Set algorithm-related parameters (N = 30)
Ensure: Read in low-illumination image
1: **while** $t < T$ (T = 50) **do**
2: Normalized image
3: Global double-gamma correction by Formula (16)
4: Denormalization
5: Calculate the fitness value of the image
6: Use HHO for optimization
7: **if** fitness(t) < fitness(t + 1) **then**
8: fitness(t + 1) = fitness(t)
9: **end if**
10: **end**

3.4. Adaptive Enhancement of Low-Illuminance Images Using the Incomplete Beta Function Based on the Improved Harris Eagle Algorithm

Different grayscale transformation functions [47] can produce different enhancement effects on images, such as grayscale transformation functions that expand darker regions, grayscale transformation functions that expand brighter regions grayscale transformation functions that stretch and compress the middle regions, and grayscale transformation functions that stretch and compress the two edge regions. Grayscale transformation functions are shown in Table 3. Tubbs proposed a normalized incomplete beta function that can automatically fit the four grayscale transformation functions mentioned above. The normalized incomplete beta function formula is as follows:

$$F(u) = B^{-1}(\alpha, \beta) \times \int_0^u t^{\alpha-1}\left(1-t\right)^{\beta-1} dt \tag{17}$$

$$B(\alpha, \beta) = \int_0^1 t^{\alpha-1}\left(1-t\right)^{\beta-1} dt \tag{18}$$

In Equations (17) and (18), α and β are two parameters, u is the normalized gray value, and t is an integral variable. In this way, various types of nonlinear grayscale change functions can be obtained by adjusting the value of the parameters. The formula for grayscale conversion using a normalized incomplete beta function is as follows:

$$T(I_{mn}) = f(I_{mn}, \alpha, \beta) = \int_0^{I_{mn}} \frac{t^{\alpha-1}(1-t)^{\beta-1}}{B(\alpha, \beta)} dt \tag{19}$$

In Equation (19), I_{mn} represents the grayscale value of the normalized $m * n$ size image. The improved Harris Hawk algorithm is used to search for the α and β of the incomplete beta function. By adjusting these two parameter values, the enhanced image is continuously iterated toward higher fitness values. The pseudocode is as follows in Algorithm 3:

Table 3. Grayscale transformation functions.

Grayscale Transformation Functions	Enhancement Effects on Images
expand	darker regions
expand	brighter regions
stretch and compress	middle regions
stretch and compress	two edge regions

Algorithm 3. Using the improved Harris Hawk algorithm and incomplete beta function to enhance a low-illumination image

Require: Set algorithm-related parameters (N = 30)
Ensure: Read in low-illumination image
1: **while** $t < T$ (T = 50) **do**
2: Normalize the image and change it into a one-dimensional vector
3: Incomplete beta enhancement of image using Formula (19)
4: Denormalization
5: Calculate the fitness value of the image
6: UseHHO for optimization
7: **if** fitness(t) < fitness(t + 1) **then**
8: fitness(t + 1) = fitness(t)
9: **end if**
10: **end**

4. Experiment

4.1. Functional Testing

This paper compared the improved Harris Eagle algorithm with the original algorithm to test the performance of the improved algorithm and then compared it with the current emerging swarm intelligence algorithms. The tuna algorithm (TSO) [48], sparrow algorithm (SSA) [49], jumping spider optimization algorithm (JSOA) [50], butterfly algorithm (BOA) [51], marine predator algorithm (MPA) [52], whale algorithm (WOA) [53], Myxomyces algorithm (SMA) [54], and tarp sheath optimization algorithm (SSOA) [55] were compared.

TSO is a novel intelligent optimization algorithm that simulates the foraging behavior of tuna populations to optimize problems and has the characteristic of fast convergence speed. SSA simulates the foraging behavior of sparrows, which utilizes many operations to avoid getting stuck in local optima and improve population diversity. JSOA provides a good balance between the development and exploration of solution search spaces and solves global optimization problems. BOA draws inspiration from the foraging and mating behavior of butterflies, utilizing fragrance, pheromones, and mutation operations for global and local searches, with the characteristic of simple implementation. MPA is an optimization algorithm that simulates the process of ocean survival, quickly seeking optimal solutions through local search and local optimal strategies. WOA is a new type of swarm intelligence optimization search method, which originated from the simulation of the hunting behavior of humpback whales. The entire process of this algorithm includes the following three stages: search and foraging, contraction and encirclement, and spiral updating of position. The inspiration for SMA comes from the predatory behavior of slime molds, which search for the optimal solution by updating individual weights and positions. SSOA searches for the optimal solution through cooperation and competition among group members, which has good robustness and adaptability and can be applied to different types of optimization problems. The above heuristic algorithms have fast convergence speed, strong search ability, good robustness, and excellent overall performance. In the experimental part of this article, the improved IHHO algorithm is compared with these advanced algorithms to highlight the better performance of the proposed algorithm.

The test functions selected were seven commonly used test functions from the standard test function set CEC 2005. The CEC 2005 benchmark test suite includes 25 testing functions. Based on the characteristics of the problems, they can be further divided into four categories as follows: unimodal problems, basic multimodal problems, extended multimodal problems, and mixed composite problems. They can test the convergence performance of the algorithm and the balance ability between global exploration and local development of the decision space. Therefore, this benchmark test suite can effectively evaluate the performance of the algorithm and is one of the most widely used and classic testing sets. The number of populations is 30, and the maximum number of iterations is

1000. The environment for this experiment is Matlab2018b, and the test platform processor is i7-1255U (1.7 GHz). The details of the test function are as follows in Table 4:

Table 4. Basic information of the test function.

Function	Dimension	Range	Minimum
$F_1 = \sum\limits_{i=1}^{n} {x_i}^2$	30	[−100, 100]	0
$F_2(x) = \sum\limits_{i=1}^{n} \lvert x_i \rvert + \prod\limits_{i=1}^{n} \lvert x_i \rvert$	30	[−10, 10]	0
$F_3(x) = \sum\limits_{i=1}^{n} \left(\sum\limits_{j-1}^{i} x_j \right)^2$	30	[−100, 100]	0
$F_4(x) = max_i\{\lvert x_i \rvert, 1 \leq x \leq n\}$	30	[−100, 100]	0
$F_5(x) = \sum\limits_{i=1}^{n} \left[{x_i}^2 - 10cos(2\pi x_i) + 10 \right]$	30	[−5.12, 5.12]	0
$F_6(x) = -20exp(-0.2\sqrt{\frac{1}{n}\sum\limits_{i=1}^{n} {x_i}^2}) - exp(\frac{1}{n}\sum\limits_{i=1}^{n} cos(2\pi x_i)) + 20 + e$	30	[−32, 32]	0
$F_7(x) = \frac{1}{4000}\sum\limits_{i=1}^{n} {x_i}^2 - \prod\limits_{i=1}^{n} cos(\frac{x_i}{\sqrt{i}}) + 1$	30	[−600, 600]	0

F1 to F4 are unimodal functions, while F5 to F7 are multimodal functions. Based on Figures 7–13, the convergence speed of the improved algorithm has been greatly improved for both unimodal and multimodal functions. In Figures 7–10, JSOA has the fastest convergence speed among the nine emerging swarm intelligence algorithms, followed by SMA and TSO. However, the convergence speed of the improved Harris Eagle algorithm surpasses them in unimodal test functions. In Figures 11–13, JSOA, SSA, TSO, MPA, and WOA all demonstrate excellent optimization capabilities, but overall, IHHO still has the fastest convergence speed and the most excellent optimization performance. The reason why IHHO exhibits excellent convergence speed is due to the improved prey energy formula and the nonlinear inertia factor in the particle swarm optimization algorithm, which can accelerate the algorithm's transformation from a global search strategy to a local search strategy and accelerate local search speed during the iteration process. HHO is suitable for a wide range of optimization problems. A hybrid improvement method is present. IHHO significantly improves the optimization of continuous problems from experimental results, especially in the processing of some unimodal functions. The improved hybrid method also performs well in multimodal functions. Table 5 compares the test results of the various algorithms.

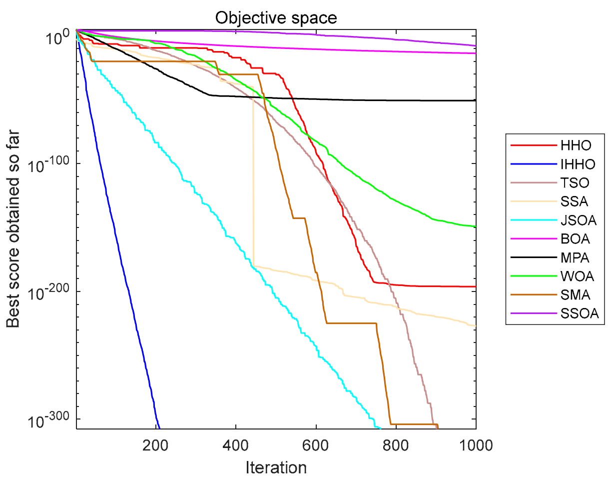

Figure 7. Convergence curve of F1.

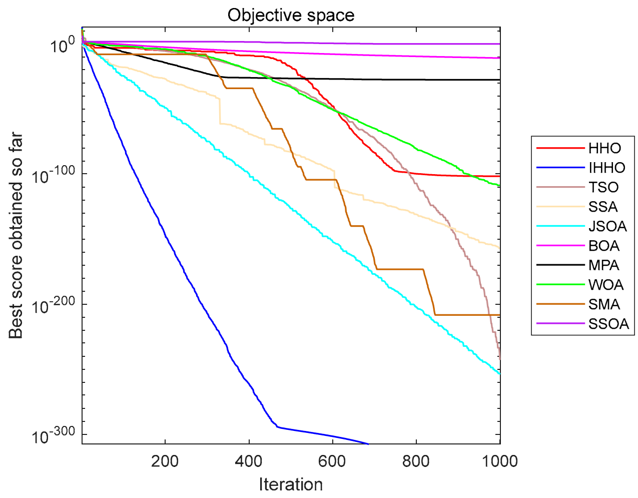

Figure 8. Convergence curve of F2.

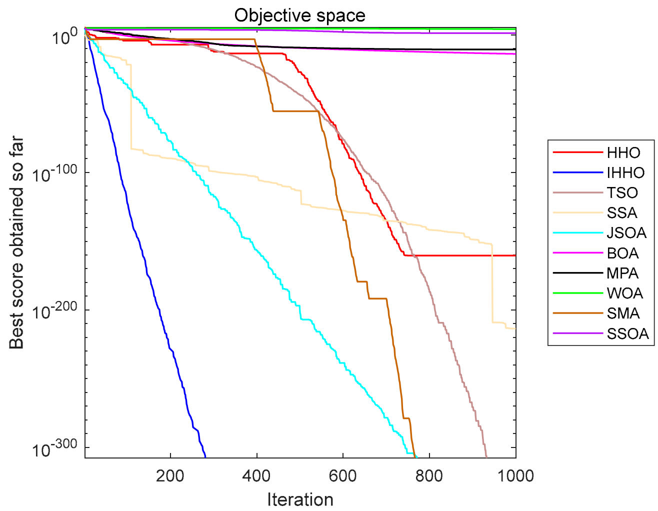

Figure 9. Convergence curve of F3.

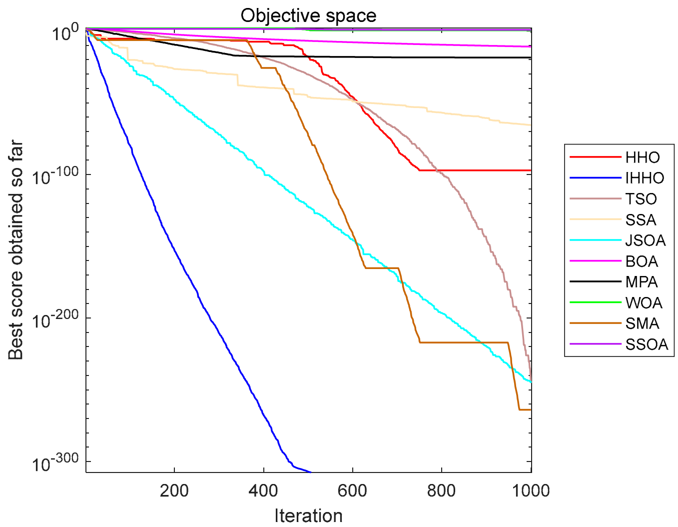

Figure 10. Convergence curve of F4.

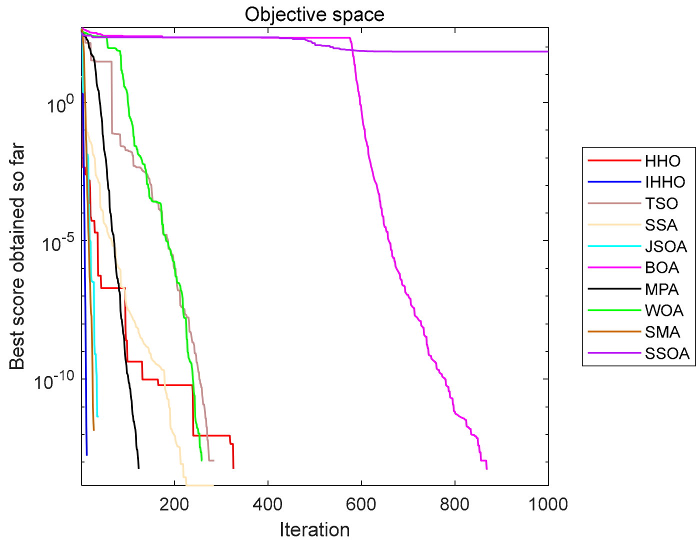

Figure 11. Convergence curve of F5.

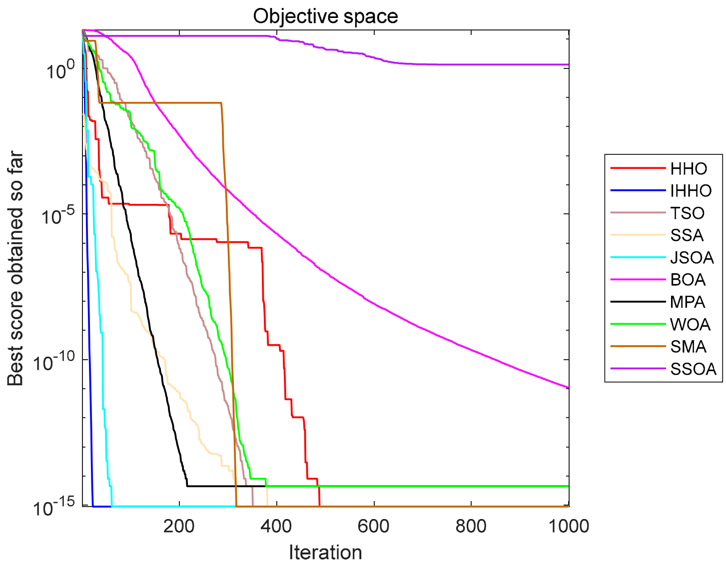

Figure 12. Convergence curve of F6.

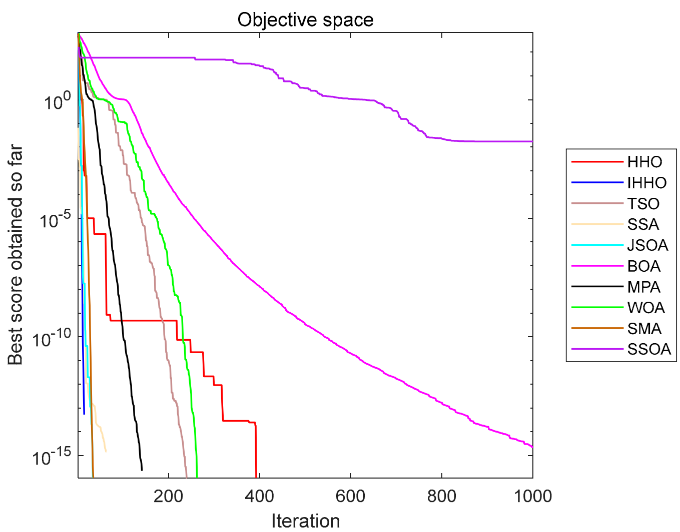

Figure 13. Convergence curve of F7.

Table 5. Test results of each algorithm.

		F1	F2	F3	F4	F5	F6	F7
HHO	best	3.1150×10^{-211}	5.9675×10^{-109}	7.1556×10^{-178}	1.0611×10^{-103}	0	8.8818×10^{-16}	0
	mean	1.1513×10^{-189}	1.9371×10^{-95}	1.3219×10^{-146}	4.5387×10^{-95}	0	8.8818×10^{-16}	0
	std	0	8.4299×10^{-95}	5.9115×10^{-146}	1.5693×10^{-94}	0	2.0234×10^{-31}	0
IHHO	best	**0**	**0**	**0**	**0**	**0**	$\mathbf{8.8818} \times 10^{-16}$	0
	mean	**0**	**0**	**0**	**0**	**0**	$\mathbf{8.8818} \times 10^{-16}$	0
	std	**0**	**0**	**0**	**0**	**0**	$\mathbf{2.0234} \times 10^{-31}$	0
TSO	best	0	2.7763×10^{-251}	0	6.9128×10^{-244}	0	8.8818×10^{-16}	0
	mean	0	1.1669×10^{-228}	0	1.3651×10^{-222}	0	8.8818×10^{-16}	0
	std	0	0	0	0	0	2.0234×10^{-31}	0
SSA	best	0	3.2666×10^{-223}	0	0	0	8.8818×10^{-16}	0
	mean	5.3221×10^{-92}	2.3238×10^{-124}	1.0403×10^{-74}	9.4200×10^{-42}	0	8.8818×10^{-16}	0
	std	2.2580×10^{-91}	1.0285×10^{-123}	4.1824×10^{-74}	4.2128×10^{-41}	0	2.0234×10^{-31}	0
JSOA	best	0	0	0	0	0	8.8818×10^{-16}	0
	mean	0	4.0251×10^{-251}	0	1.5087×10^{-247}	0	8.8818×10^{-16}	0
	std	0	0	0	0	0	2.0234×10^{-31}	0
BOA	best	1.5105×10^{-14}	2.7026×10^{-12}	1.5180×10^{-14}	1.0503×10^{-11}	0	3.2339×10^{-12}	0
	mean	1.7872×10^{-14}	1.0193×10^{-11}	1.7741×10^{-14}	1.2049×10^{-11}	20.5156	1.2001×10^{-11}	2.1316×10^{-15}
	std	1.0932×10^{-15}	2.5939×10^{-12}	1.2703×10^{-15}	6.4790×10^{-13}	59.1436	2.1933×10^{-12}	1.6391×10^{-15}
MPA	best	1.1239×10^{-51}	7.9576×10^{-30}	1.9301×10^{-19}	3.4795×10^{-20}	0	8.8818×10^{-16}	0
	mean	3.7722×10^{-50}	6.0506×10^{-28}	9.1105×10^{-12}	2.3215×10^{-19}	0	4.0856×10^{-15}	0
	std	3.7781×10^{-50}	1.2852×10^{-27}	4.0200×10^{-11}	1.5989×10^{-19}	0	1.0935×10^{-15}	0
WOA	best	1.3718×10^{-168}	1.5552×10^{-114}	152.2944	0.1975	0	8.8818×10^{-16}	0
	mean	1.6648×10^{-148}	1.8893×10^{-101}	2.2701×10^{4}	38.6550	2.8421×10^{-15}	4.7962×10^{-15}	0
	std	7.4452×10^{-148}	8.4374×10^{-101}	1.2968×10^{4}	26.3268	1.2710×10^{-14}	2.5515×10^{-15}	0
SMA	best	0	0	0	0	0	8.8818×10^{-16}	0
	mean	0	8.2035×10^{-202}	0	2.4372×10^{-184}	0	8.8818×10^{-16}	0
	std	0	0	0	0	0	2.0234×10^{-31}	0
SSOA	best	5.8679×10^{-9}	8.3940×10^{-4}	54.5625	5.1065	31.8387	1.1551	4.5420×10^{-8}
	mean	1.1892×10^{-8}	1.2820	286.5403	7.5636	61.0406	2.2548	0.0073
	std	3.2202×10^{-9}	2.7615	168.6921	2.4589	20.6527	0.5109	0.0092

The high accuracy of the IHHO results is due to the improvement in the global search strategy of HHO resulting from the spiral motion of BWO. In addition, the optimized prey energy formula and the modified Levy strategy have both improved the accuracy of HHO. JSOA is a new type of swarm intelligence algorithm inspired by the idea of the black widow algorithm. It performs very well in test results, finding the optimal value in the results of multiple test functions. Next are the tuna algorithm and slime fungus algorithm. The tuna algorithm is a heuristic algorithm newly proposed in 2021, which can quickly seek optimization by relying on two strategies, i.e., spiral feeding and parabolic feeding, and has a convergence speed and result accuracy of the optimal value. This was verified by the convergence image and test results above. The slime mold algorithm has a wide range of applications in many fields and is characterized by high accuracy. Compared with these algorithms, the traditional Harris Hawk algorithm does not have an advantage, but the IHHO changed this situation, making it comprehensively superior to the current emerging swarm intelligence algorithms in terms of both accuracy and convergence speed.

4.2. Contrast Experiment of Low-Illuminance Image Enhancement

This article proposes an improved heuristic algorithm combined with a correction function for a low-illumination image enhancement strategy. The objective is to use the combination of optimized correction parameters to optimize the best fitness value. First, random low-illumination image information is input, and the image is preprocessed and normalized. Then, the relevant parameters of the intelligent algorithm (specific parameter information is shown in Table 6) are initialized with the image entropy value as the objective function, and then the improved heuristic algorithm in Section 3 is used to solve it to obtain the best parameter combination of the incomplete β correction function and the double gamma correction function, which is used to globally correct the image based on the parameter combination information. Finally, the image information is normalized, and the enhanced image effect is output. Since this adaptive method of determining parameters through intelligent algorithms does not require training, it can effectively prevent under-enhancement and over-enhancement while saving computational resources. The algorithm parameter values used in the experiment are shown in Table 6.

Table 6. The algorithm parameter values used in the experiment.

Parameters	**Values**
α_1	5
β_1	1
α_3	0.01
β_3	1.5
N	30
T	50
T_0	1000
w_start	0.9
w_end	0.4

This paper used the LOL dataset to test several images enhancement methods to study the performance of IHHO in low-illumination image enhancement. The images in LOL data are all taken from a real environment and are part of a dataset containing many real scene images. This dataset preserves the characteristics and attributes under real conditions and is widely used in image enhancement research. Our research and testing methods include contrast-limited adaptive histogram equalization (CLAHE), single scale Retinex enhancement (SSR), homomorphic filtering, and the proposed IHHO and gamma-corrected adaptive image enhancement (IHHO-BIGA) and IHHO and incomplete beta adaptive image enhancement (IHHO-NBeta). IHHO-BIGA and IHHO-Nbeta are two adaptive image enhancement methods proposed in this study that utilize swarm intelligence algorithms with correction functions. The population number is set to 30, and the maximum number of iterations is set to 50. The corresponding search dimension is set based on the correction function. The enhancement results of various algorithms for low-illumination images and their corresponding grayscale histograms are in the following order: low-illumination source image, CLAHE method, SSR method, homomorphic filtering method, IHHO-BIGA, and IHHO-NBeta. In the following figure, a represents the processed image and b represents the grayscale histogram.

The enhancement effects of the three methods shown in Figure 14, including CLAHE, SSR, and homomorphic filtering, are average. The enhancement in dark areas is not obvious but highlights the details of the red carpet. IHHO-BIGA and IHHO-Nbeta have the most obvious enhancement effects on low-illumination images of audience seats, but the enhanced IHHO-Nbeta images have richer and more prominent details, and fewer noise points appear.

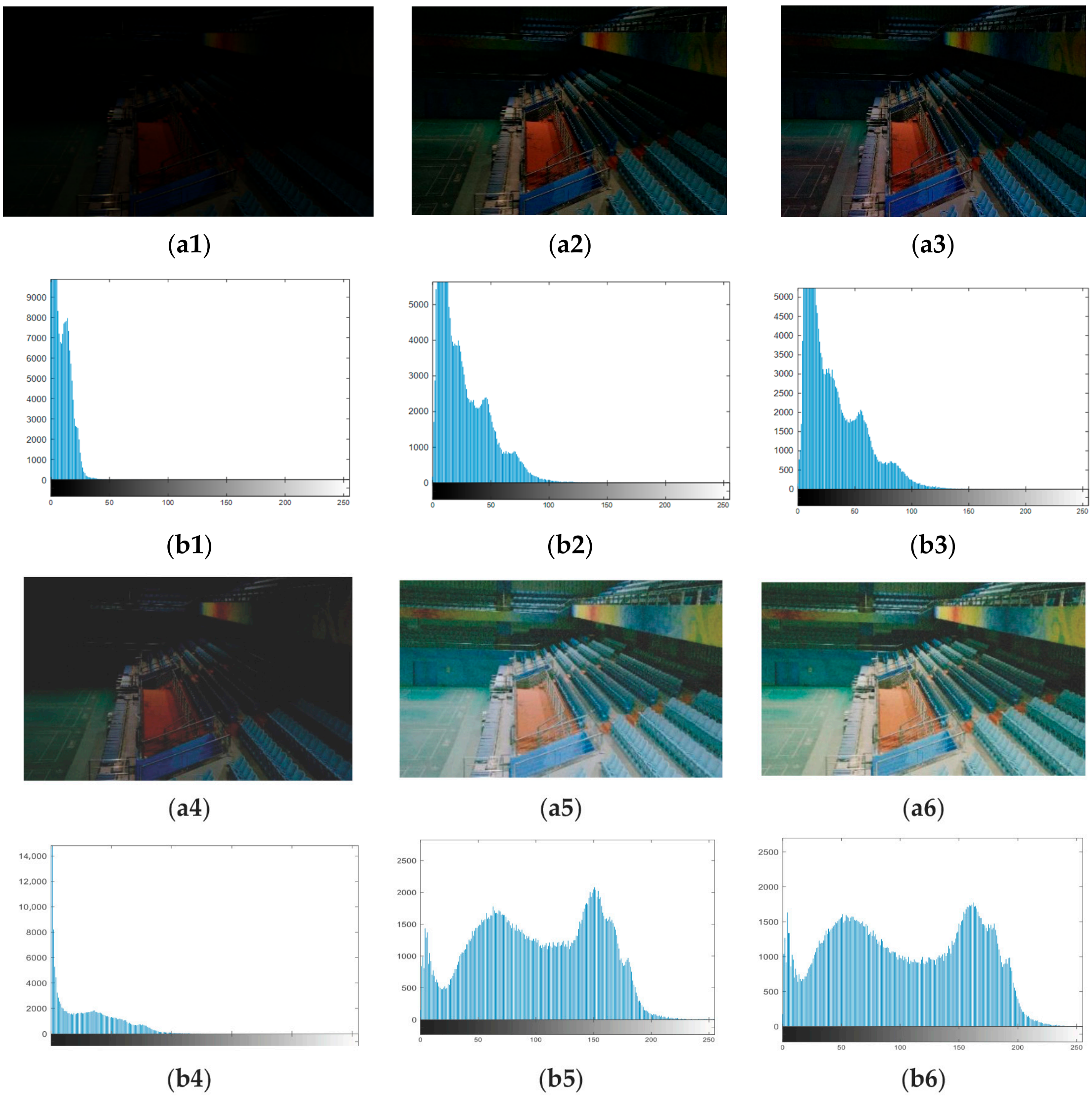

Figure 14. Enhancement results of various algorithms on the low-illumination image numbered 778 and their corresponding grayscale histograms. (**a1**,**b1**) S-image. (**a2**,**b2**) CLAHE. (**a3**,**b3**) SSR. (**a4**,**b4**) H-f. (**a5**,**b5**) IHHO-BIGA. (**a6**,**b6**) IHHO-NBeta.

Figure 15 shows the low-illumination image enhancement of a number plate, where CLAHE has the worst enhancement effect with many dark areas not enhanced, and the image contrast is also very low. Both the SSR and homomorphic filtering methods highlight some details, such as the red light above the image and the bright area on the left, but the overall brightness of the image is not high. IHHO-BIGA and IHHO-Nbeta enhance the overall brightness of the low-illumination number plate images, resulting in a significant improvement in the image information.

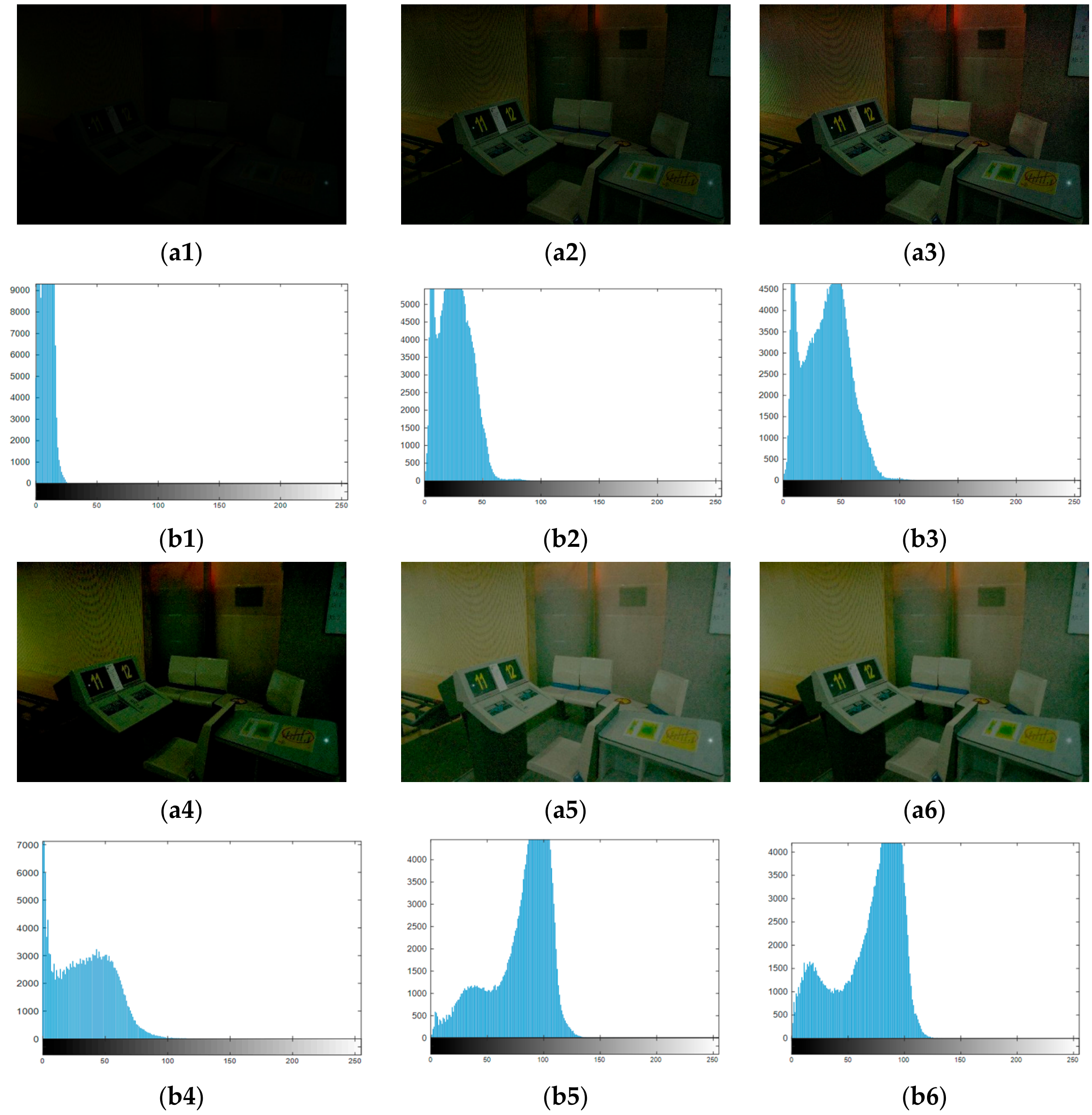

Figure 15. Enhancement results of various algorithms on the low-illumination image numbered 665 and their corresponding grayscale histograms. (**a1**,**b1**) S-image. (**a2**,**b2**) CLAHE. (**a3**,**b3**) SSR. (**a4**,**b4**) H-f. (**a5**,**b5**) IHHO-BIGA. (**a6**,**b6**) IHHO-NBeta.

Figure 16 shows the enhancement of the image of a climbing site. It can be intuitively seen that the enhancement effects of CLAHE and SSR are very general. Although homomorphic filtering highlights some details, such as light highlights, the overall image shows insufficient exposure and low contrast. Although IHHO-BIGA greatly improved the brightness and contrast, there is still an overall underexposure situation. Compared with this, the enhancement effect of IHHO-Nbeta on rock climbing sites is more eye-catching, not only enhancing multiple dark places but also retaining rich details, without any exposure or underexposure.

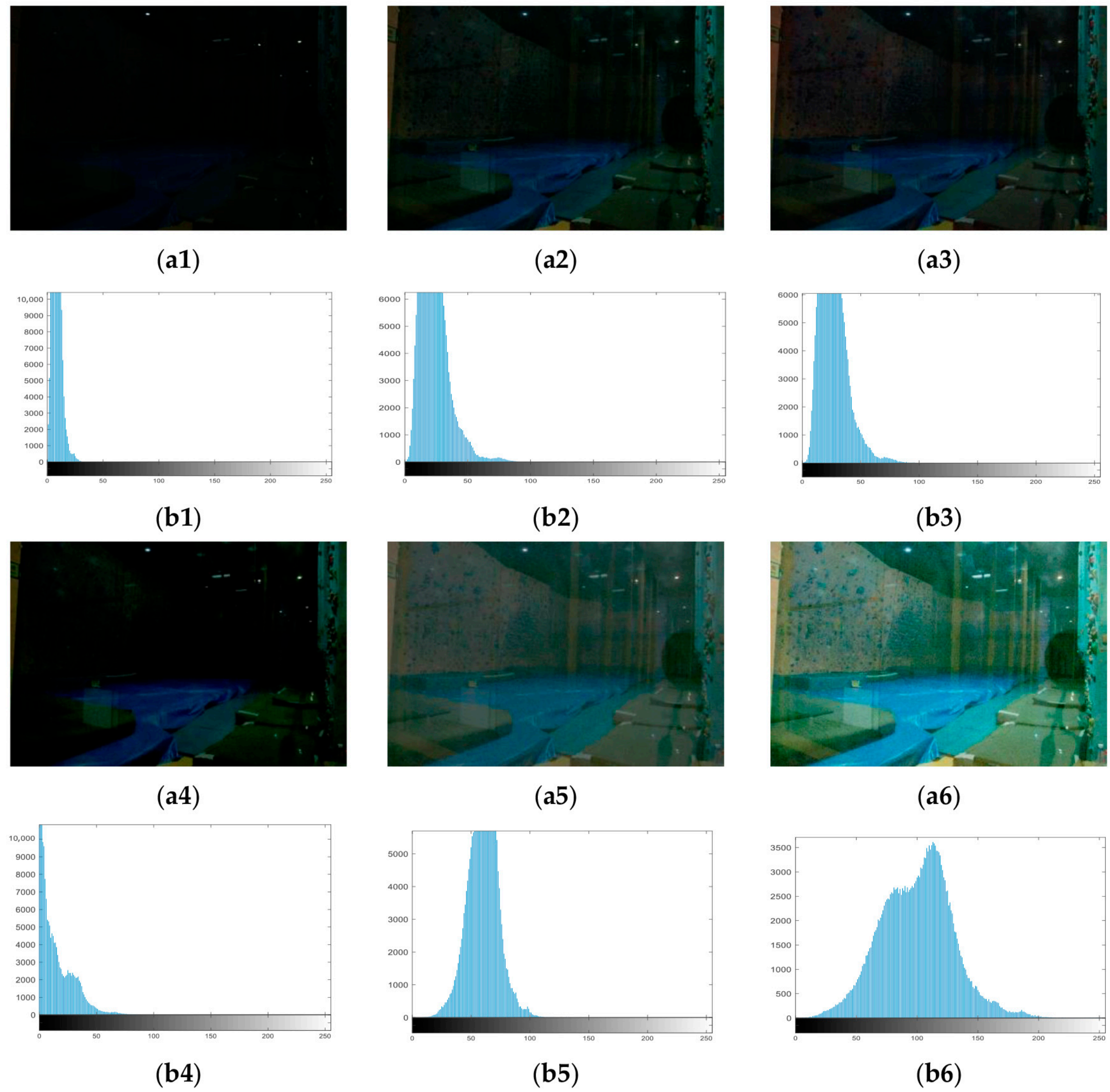

Figure 16. Enhancement results of various algorithms on the low-illumination image numbered 757 and their corresponding grayscale histograms. (**a1**,**b1**) S-image. (**a2**,**b2**) CLAHE. (**a3**,**b3**) SSR. (**a4**,**b4**) H-f. (**a5**,**b5**) IHHO-BIGA. (**a6**,**b6**) IHHO-Nbeta.

Figure 17 shows the enhancement of a low-illumination image of a swimming pool. CLAHE, SSR, and homomorphic filtering all provide better-detailed information than IHHO-BIGA. Although using IHHO-BIGA to enhance a low-illumination image of a swimming pool improves brightness to some extent, the contrast is poor. The enhancement effect using IHHO-Nbeta is excellent, not only effectively suppressing noise but also further improving image quality in terms of contrast, brightness, and detail information.

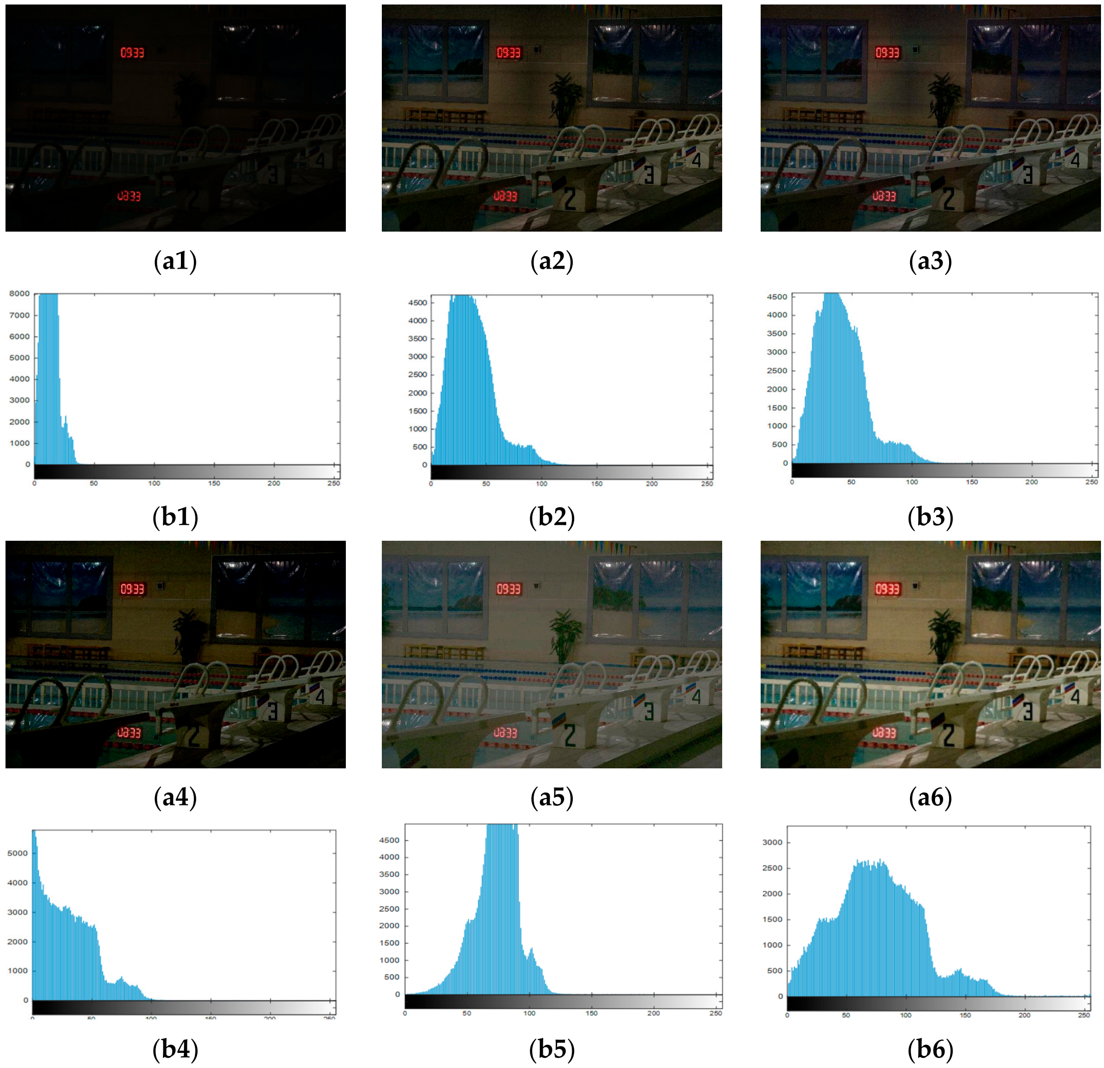

Figure 17. Enhancement results of various algorithms on the low-illumination image numbered 748 and their corresponding grayscale histograms. (**a1**,**b1**) S-image. (**a2**,**b2**) CLAHE. (**a3**,**b3**) SSR. (**a4**,**b4**) H-f. (**a5**,**b5**) IHHO-BIGA. (**a6**,**b6**) IHHO-NBeta.

Figure 18 shows the enhancement of low-illumination images in a table tennis room. It can be seen that homomorphic filtering has a significant improvement effect on the image, not only improving the brightness to a certain extent but also resulting in high contrast. However, compared with the latter two methods, CLAHE, SSR, and homomorphic filtering have a weaker improvement in brightness. During the process of image enhancement in the table tennis room by IHHO-BIGA, there was a phenomenon of insufficient exposure, and some detailed information was not presented in place. The enhancement effect of IHHO-Nbeta on the table tennis room image is the most outstanding, which is also the most intuitive visual experience. It not only highlights some detailed information such as lighting and wooden frames but also has a very intuitive enhancement effect on brightness and contrast. Based on the results of the grayscale histogram, compared with the other methods, IHHO-Nbeta has a more uniform grayscale distribution, which has an excellent enhancement effect.

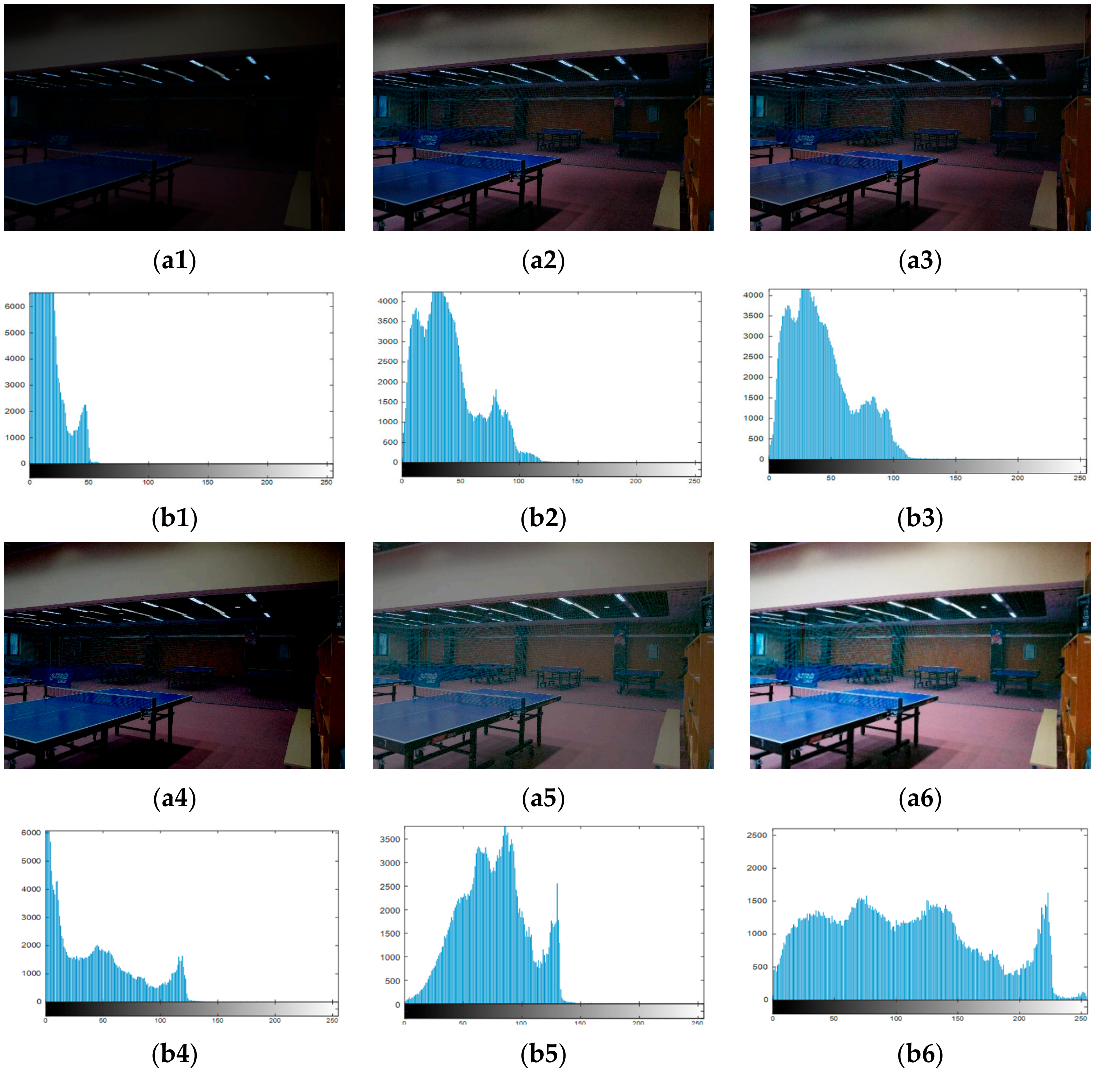

Figure 18. Enhancement results of various algorithms on the low-illumination image numbered 760 and their corresponding grayscale histograms. (**a1**,**b1**) S-image. (**a2**,**b2**) CLAHE. (**a3**,**b3**) SSR. (**a4**,**b4**) H-f. (**a5**,**b5**) IHHO-BIGA. (**a6**,**b6**) IHHO-NBeta.

This paper also used five evaluation indicators, namely, the average gradient (AG), standard deviation (SD), spatial frequency (SF), information entropy (IE), and correlation coefficient (CC), to measure the enhancement effect of each method. The average gradient refers to the difference in gray levels near the edge or both sides of the shadow line of an image, reflecting the clarity and texture changes in the image. The larger the average gradient, the clearer the image. The standard deviation represents the degree of dispersion of gray levels relative to the mean value of gray levels and is commonly used to evaluate the contrast of an image. The larger the standard deviation, the more prominent and clear the image details are. Spatial frequency refers to the rate of change in the gray scale of an image, reflecting the overall activity of the spatial domain of an image. The higher the spatial frequency, the clearer the image. Information entropy is the most used image evaluation index, which measures the amount of information contained in an image. The greater the entropy, the more information it contains. This paper also uses correlation coefficients as evaluation indicators to verify the difference in and relationship between the enhanced image and the highlighted image. The correlation coefficients reflect the correlation between the two images. The larger the correlation coefficients, the higher the similarity between the two images.

$$AG = \frac{1}{(M)(N)} \sum_{i=1}^{M} \sum_{j=1}^{N} \sqrt{\frac{(\nabla_x I(i,j))^2 + (\nabla_y I(i,j))^2}{2}} \tag{20}$$

In Equation (20), $(\nabla_x I(i,j))$ represents the horizontal gradient and $(\nabla_y I(i,j))$ represents the vertical gradient.

$$SD = \sqrt{\frac{1}{M \times N} \sum_{i=1}^{M} \sum_{j=1}^{N} (P(i,j) - \mu)^2} \tag{21}$$

In Equation (21), $P(i,j)$ represents the pixel value and μ represents the mean value.

$$SF = \sqrt{RF^2 + CF^2} RF = \sqrt{\sum_{i=1}^{M} \sum_{j=1}^{N} (F(i,j) - F(i,j-1))^2}$$

$$CF = \sqrt{\sum\nolimits_{i=1}^{M} \sum\nolimits_{j=1}^{N} (F(i,j) - F(i-1,j))^2} \tag{22}$$

In Equation (22), $F(i,j)$ represents the values of pixels in the i-th row and the j-th column of the fused image.

$$IE = -\sum\nolimits_{n=0}^{N-1} p_n log_2 p_n \tag{23}$$

In Formula (23), N represents the gray level of the fused image and p_n represents the normalized histogram of the corresponding gray level in the fused image.

$$CC(I_H, I_W) = \frac{\sum_{i=1}^{M} \sum_{j=1}^{N} \left(I_H(i,j) - \overline{I_H}\right)\left(I_W(i,j) - \overline{I_W}\right)}{\sqrt{\sum_{i=1}^{M} \sum_{j=1}^{N} \left(I_H(i,j) - \overline{I_H}\right)^2 \times \sum_{i=1}^{M} \sum_{j=1}^{N} \left(I_w(i,j) - \overline{I_w}\right)^2}} \tag{24}$$

In Equation (24), $\overline{I_H}$ and $\overline{I_w}$ are the pixel averages of the fused image and the ideal reference image, respectively. In the following tables, S-image represents the original image, CLAHE represents the limited contrast adaptive histogram equalization method, SSR represents the single-scale Retinex enhancement method, H-f represents the homomorphic filtering method, Method1 refers to IHHOBIGA proposed in this study, and Method2 refers to IHHO-NBeta proposed in this study.

Based on Table 7, the various evaluation indicators of IHHO-Nbeta are the highest, with both IHHO-BIGA and IHHO-Nbeta having relatively high AG indicators. This indicates that the correction function adaptive enhancement method optimized by the two population intelligent algorithms proposed in this article has a significant enhancement effect on the clarity of low-illumination images in the audience. The standard deviation data results also show that these two methods highlight the details of the image. The data of SSR and homomorphic filtering are close in terms of standard deviation, spatial frequency, and the correlation coefficient, which are significantly different from the two methods proposed in this article. The standard deviation of IHHO-Nbeta increased by 8.26% compared with IHHO-BIGA and increased by 120.91% compared with SSR. From the perspective of information entropy, the difference between IHHO-BIGA and IHHO-Nbeta is not significant, indicating that the information content displayed by the two is similar. The information entropy of the image enhanced using IHHO-BIGA is 76.84% higher than the original image. From the perspective of the correlation coefficient, the value of IHHO-Nbeta is closest to 1, indicating that the enhancement result of this method for low-illumination images is closest to that of high-brightness images.

Table 7. Low-illumination image enhancement evaluation index data numbered 778.

	AG	SD	SF	IE	CC
S-image	3.1702	8.1606	6.5411	4.3397	0.8975
CLAHE	6.2416	23.3295	15.5480	6.0138	0.8843
ssr	7.0360	27.8816	17.3021	6.2577	0.8834
H-f	6.3814	27.1519	18.9249	4.4692	0.8458
IHHO-BIGA	19.9441	56.8938	38.0151	7.6334	0.9092
IHHO-Nbeta	**21.2186**	**61.5943**	**40.1471**	**7.6742**	**0.9213**

Based on Table 8, homomorphic filtering, IHHO-BIGA, and IHHO-Nbeta have excellent enhancement data for low-illumination images of number plates, while CLAHE and SSR have average enhancement effects on the images. Among them, the homomorphic filtering method exhibits the highest average gradient value and spatial frequency value, which indicates that the sharpness of the low-illumination image of the number plate has been greatly improved after homomorphic filtering. However, the standard deviation, information entropy, and correlation coefficient of the homomorphic filtering method are not as high as IHHO-BIGA and IHHO-Nbeta, which indicates that the homomorphic filtering method is not as good as the two methods proposed in this article in terms of contrast and detail performance. At the same time, IHHO-Nbeta exhibits the highest standard deviation, information entropy, and correlation coefficient values, indicating that using IHHO-Nbeta for enhancement is the best. The standard deviation data of IHHO-Nbeta is 4.69% higher than that of IHHO-BIGA, and 25.57% higher than that of homomorphic filtering. The information entropy of the number plate image enhanced by IHHO-Nbeta increased by 59.01% compared with the original image with low illumination.

Table 8. Low-illumination image enhancement evaluation index data numbered 665.

	AG	SD	SF	IE	CC
S-image	2.7434	5.3244	3.7491	4.2579	0.8696
CLAHE	3.7611	14.7350	7.4791	5.7686	0.8172
ssr	5.8038	20.4278	11.1222	6.2590	0.8748
H-f	**8.2414**	24.8869	**15.4647**	5.3619	0.7709
IHHO-BIGA	7.4097	29.8503	14.7174	6.7349	0.9192
IHHO-Nbeta	7.3122	**31.2504**	13.9868	**6.7703**	**0.9228**

Based on Table 9, the correlation coefficient value of SSR is the highest, and compared with the homomorphic filtering and CLAHE methods, SSR has a relatively good enhancement effect on rock climbing site images. However, compared with the latter two methods, there is still a significant gap. In addition to the correlation coefficient, the enhanced image indicators of IHHO-Nbeta are the best, displaying the highest clarity, contrast, detail prominence, and brightness. The standard deviation of the image enhanced by IHHO-Nbeta is 113.91% higher than that of IHHO-BIGA and 138.60% higher than that of homomorphic filtering, and the information entropy of the enhanced image is 71.47% higher.

Based on Tables 10 and 11, IHHO-Nbeta has the highest evaluation indicators for the five low-illumination images after enhancement and has significant data advantages over the previous four methods, especially in terms of average gradient, standard deviation, and spatial frequency. This also proves that using IHHO-Nbeta to enhance low-illumination images provides significant improvements in image texture clarity, contrast, detail performance, and brightness. In the low-illumination image enhancement process of the swimming pool and table tennis room, the 16 standard deviations of IHHO-Nbeta compared with the homomorphic filtering method increased by 55.80% and 63.02%, respectively. The information entropy of the enhanced image increased by 51.03% and 44.02%, respectively.

Table 9. Low-illumination image enhancement evaluation index data numbered 757.

	AG	SD	SF	IE	CC
S-image	2.5104	6.4304	4.6213	4.3429	0.8536
CLAHE	2.9167	16.2350	6.5828	5.7731	0.8962
ssr	3.1696	15.8214	6.7094	5.7996	**0.9243**
H-f	2.0652	18.3787	7.1302	4.1899	0.8285
IHHO-BIGA	4.4760	20.5003	8.2642	6.3395	0.8842
IHHO-Nbeta	**12.2920**	**43.8519**	**21.4519**	**7.4467**	0.8925

Table 10. Low-illumination image enhancement evaluation index data numbered 748.

	AG	SD	SF	IE	CC
S-image	3.6233	10.0421	9.3485	4.7943	0.7949
CLAHE	5.7452	21.5673	12.9745	6.2995	0.8961
ssr	5.7954	22.0931	13.4155	6.3678	0.8933
H-f	6.4745	25.1076	15.7843	5.8584	0.8919
IHHO-BIGA	4.9597	20.3172	11.6035	6.2909	0.9257
IHHO-Nbeta	**10.5824**	**39.1181**	**22.6541**	**7.2409**	**0.9430**

Table 11. Low-illumination image enhancement evaluation index data numbered 760.

	AG	SD	SF	IE	CC
S-image	3.5139	15.9728	11.2243	5.4324	0.9257
CLAHE	5.7343	28.9035	15.1955	6.6614	0.9310
ssr	5.6648	28.7513	15.0870	6.6752	0.9341
H-f	5.4220	39.8834	17.9716	6.2036	**0.9698**
IHHO-BIGA	6.4993	31.3341	16.4246	6.9233	0.9579
IHHO-Nbeta	**12.5877**	**65.0176**	**29.8398**	**7.8238**	0.9663

This paper compared the processing time of the method in the text to further verify the superior performance of the proposed method. This paper did not compare them in the experiment because of the average low-illumination image enhancement effect of traditional methods and the short processing time. The comparison of processing time emphasizes the improvement brought by the heuristic hybrid optimization method proposed in this article before and after.

The optimization method using heuristic algorithms combined with dual gamma correction has a slightly shorter processing time than the incomplete beta, as shown in Table 12. The method proposed in this article takes longer than traditional methods partly because the heuristic algorithm takes some time to optimize the fitness function iteratively and partly because of the combination of correction functions to optimize the optimal parameter combination. IHHO-BIGA and IHHO-Nbeta shortened the corresponding time compared with the previous HHO without improvement thanks to the improvement in the algorithm solving speed through optimization methods such as PSO's inertia weight factor. This paper selected image 760 as an example, which performed the best in the previous experiment. IHHO-Nbeta and IHHO-BIGA reduced the processing time by 6.32% and 15.83%, respectively, compared with that before improvement. There is still a certain gap in processing time compared with the traditional image enhancement methods, although the processing time of the proposed method significantly improved compared with the previous heuristic algorithms. Our future research will focus on further speeding up the processing time for image enhancement.

Table 12. Comparison of processing time of the methods proposed in this article (in seconds).

	HHO-BIGA	HHO-Nbeta	IHHO-BIGA	IHHO-Nbeta
Image 778	104.6218	123.3315	91.4637	121.7633
Image 665	120.4861	137.3496	99.4199	133.9149
Image 757	115.6043	128.1015	109.4023	123.7776
Image 748	109.7199	126.6448	93.0412	119.8669
Image 760	110.1762	155.1992	95.1130	145.9654

5. Conclusions

This research proposes an improved Harris Hawk algorithm combined with a gamma correction function and incomplete beta function for adaptive image enhancement, which can effectively improve the shortcomings of low-illumination images such as low brightness, poor contrast, and excessive noise. In this paper, several parts of the Harris Hawk algorithm have been improved, which not only enriches the population and enhances the search ability of the Harris Hawk, but also effectively speeds up the conversion between global search and local search, improves the convergence speed of the algorithm, and maintains better algorithm accuracy. The improvement measures proposed in this study can make the Harris Eagle algorithm stand out among many emerging algorithms and achieve the most excellent performance. IHHO-Nbeta proposed in this article has shown the best results in low-illumination image enhancement results from multiple LOL datasets. It can not only improve the brightness and contrast of low-illumination images but also effectively overcomes noise and avoids color distortion. The comparison methods include CLAHE, SSR, homomorphic filtering, and IHHO-BIGA. The method of combining heuristic algorithms with correction functions for low-illumination image enhancement does not have an advantage in processing time compared to traditional methods. Our future work will focus on accelerating the processing time of image enhancement. We will continue to explore methods of fusing other image enhancement in our future research. The method proposed in this study is expected to have good reference significance and practical application effects in underwater photography applications, medical images, remote sensing images, and meteorological image fog removal because of the many application fields of low-illumination image enhancement. Our future work will also focus on the above areas.

Author Contributions: Conceptualization, Y.Z. and Y.L.; methodology, Y.L.; software, Y.L.; validation, Y.Z. and X.L.; formal analysis, X.L.; investigation, Y.Z.; resources, Y.L.; data curation, X.L.; writing—original draft preparation, Y.L.; writing—review and editing, Y.L.; visualization, Y.Z.; supervision, X.L.; project administration, Y.Z.; funding acquisition, Y.Z. All authors have read and agreed to the published version of the manuscript.

Funding: This work was supported by the fund of the Science and Technology Development Project of Jilin Province, No. 20220203190SF, and the fund of the education department of Jilin Province, No. JJKH20210257KJ.

Data Availability Statement: The original contributions presented in this study are included in this article. Further inquiries can be directed to the corresponding author.

Conflicts of Interest: The authors declare that this research was conducted in the absence of any commercial or financial relationships that could be construed as a potential conflict of interest.

References

1. Sun, K.; Tian, Y. Dbfnet: A dual-branch fusion network for underwater image enhancement. *Remote Sens.* **2023**, *15*, 1195. [CrossRef]
2. Guo, X.; Yang, Y.; Wang, C.; Ma, J. Image dehazing via enhancement, restoration, and fusion: A survey. *Inf. Fusion* **2022**, *86–87*, 146–170. [CrossRef]
3. Chen, J.; Yang, N.; Pan, Y.; Liu, H.; Zhang, Z. Synchronous medical image augmentation framework for deep learning-based image segmentation. *Comput. Med. Imaging Graph.* **2023**, *104*, 102161. [CrossRef]
4. Paul, A.; Bhattacharya, P.; Maity, S.P. Histogram modification in adaptive bi-histogram equalization for contrast enhancement on digital images. *Optik* **2022**, *259*, 168899. [CrossRef]

5. Wang, W.; Sun, N.; Ng, M.K. A variational gamma correction model for image contrast enhancement. *Inverse Probl. Imaging* **2019**, *13*, 461–478. [CrossRef]
6. Zhou, C.; Yang, X.; Zhang, B.; Lin, K.; Xu, D.; Guo, Q.; Sun, C. An adaptive image enhancement method for a recirculating aquaculture system. *Sci. Rep.* **2017**, *7*, 6243. [CrossRef]
7. Singh, P.; Bhandari, A.K.; Kumar, R. Naturalness balance contrast 17 enhancement using adaptive gamma with cumulative histogram and median filtering. *Optik* **2022**, *251*, 168251. [CrossRef]
8. XXia, K.J.; Yin, H.S.; Rong, G.S.; Wang, J.Q.; Jin, Y. X-ray image enhancement base on the improved adaptive low-pass filtering. *J. Med. Imaging Health Inform.* **2018**, *8*, 1342–1348. [CrossRef]
9. Gamini, S.; Kumar, S.S. Homomorphic filtering for the image enhancement based on fractional-order derivative and genetic algorithm. *Comput. Electr. Eng.* **2023**, *106*, 108566. [CrossRef]
10. Al-Shakhrah, I.A. Digital high-pass filters with milder high-pass effect on digital images. *Am. J. Eng. Appl. Sci.* **2015**, *8*, 360. [CrossRef]
11. Liu, J.; Peng, Y. Research on image enhancement algorithm based on artificial intelligence. *J. Phys. Conf. Ser.* **2021**, *2074*, 012024. [CrossRef]
12. Sheikh, I.M.; Chachoo, M.A. A novel cell image fusion approach based on the collaboration of multilevel latent low-rank representation and the convolutional neural network. *Biomed. Signal Process. Control.* **2023**, *83*, 104654.
13. Kang, S.M.; Moo, H.K.; Bok, J.Y. Detection system using eyeglasses reflection removal technique by applying color channels and ssr. *J. Inst. Control. Robot. Syst.* **2018**, *24*, 1128–1133. [CrossRef]
14. Hu, K.; Zhang, Y.; Lu, F.; Deng, Z.; Liu, Y. An underwater image enhancement algorithm based on msr parameter optimization. *J. Mar. Sci. Eng.* **2020**, *8*, 741. [CrossRef]
15. Wei, B.; Li, L. Multiscale retinex color restoration with adaptive gamma correction for foggy imageenhancement. *J. Flow Vis. Image Process.* **2021**, *28*, 71–88. [CrossRef]
16. Roslin, A.; Marsh, M.; Piché, N.; Provencher, B.; Mitchell, T.R.; Onederra, I.A.; Leonardi, C.R. Processing of micro-ct images of granodiorite rock samples using convolutional neural networks (cnn), part i: Super resolution enhancement using a 3d cnn. *Miner. Eng.* **2022**, *188*, 107748. [CrossRef]
17. Zhang, R.; Lu, W.; Gao, J.; Tian, Y.; Wei, X.; Wang, C.; Li, X.; Yu, M. Rfi-gan: A reference-guided fuzzy integral network for ultrasound image augmentation. *Inf. Sci.* **2023**, *623*, 709–728. [CrossRef]
18. Jiang, Z.; Li, H.; Liu, L.; Men, A.; Wang, H. A switched view of retinex: Deep self-regularized low light image enhancement. *Neurocomputing* **2021**, *454*, 361–372. [CrossRef]
19. Mahapatra, S.; Agrawal, S. An optimal statistical feature-based transformation function for enhancement of retinal images using adaptive enhanced leader particle swarm optimization. *Int. J. Imaging Syst. Technol.* **2022**, *32*, 2163–2183. [CrossRef]
20. Thangavel, K.; Manavalan, R. Soft computing models based feature selection for trus prostate cancer image classification. *Soft Comput.* **2014**, *18*, 1165–1176. [CrossRef]
21. Suresh, S.; Lal, S. Modified differential evolution algorithm for contrast and brightness enhancement of satellite images. *Appl. Soft Comput.* **2017**, *61*, 622–641. [CrossRef]
22. Dinh, P.H.; Giang, N.L. A new medical image enhancement algorithm using adaptive parameters. *Int. J. Imaging Syst. Technol.* **2022**, *32*, 2198–2218. [CrossRef]
23. Nasef, M.M.; Eid, F.T.; Sauber, A.M. Skeletal scintigraphy image enhancement based neutrosophic sets and salp swarm algorithm. *Artif. Intell. Med.* **2020**, *109*, 101953. [CrossRef] [PubMed]
24. Wei, C.; Wang, W.; Yang, W.; Liu, J. Deep retinex decomposition for low-light enhancement. *arXiv* **2018**, arXiv:1808.04560.
25. Rahman, H.; Paul, G.C. Tripartite sub-image histogram equalization for slightly low contrast gray-tone image enhancement. *Pattern Recognit.* **2023**, *134*, 109043. [CrossRef]
26. Zarie, M.; Parsayan, A.; Hajghassem, H. Image contrast enhancement using triple clipped dynamic histogram equalisation based on standard deviation. *IET Image Process.* **2019**, *13*, 1081–1089. [CrossRef]
27. Gupta, B.; Agarwal, T.K. Linearly quantile separated weighted dynamic histogram equalization for contrast enhancement. *Comput. Electr. Eng.* **2017**, *62*, 360–374. [CrossRef]
28. Sule, O.O.; Ezugwu, A.E. A two-stage histogram equalization enhancement scheme for feature preservation in retinal fundus images. *Biomed. Signal Process. Control* **2023**, *80*, 104384. [CrossRef]
29. Lu, P.; Huang, Q. Robotic weld image enhancement based on improved bilateral filtering and clahe algorithm. *Electronics* **2022**, *11*, 3629. [CrossRef]
30. Jeon, J.J.; Park, T.H.; Eom, I.K. Sand-dust image enhancement using chromatic variance consistency and gamma correction-based dehazing. *Sensors* **2022**, *22*, 9048. [CrossRef]
31. Lee, Y.; Zhang, S.; Li, M.; He, X. Blind inverse gamma correction with maximized differential entropy. *Signal Process.* **2022**, *193*, 108427. [CrossRef]
32. Liu, S.; Long, W.; Li, Y.; Cheng, H. Low-light image enhancement based on membership function and gamma correction. *Multimed. Tools Appl.* **2021**, *81*, 22087–22109. [CrossRef]
33. Singh, H.; Kumar, A.; Balyan, L.K.; Singh, G.K. Swarm intelligence optimized piecewise gamma corrected histogram equalization for dark image enhancement. *Comput. Electr. Eng.* **2017**, *70*, 462–475. [CrossRef]

34. Das, A.; Dhal, K.G.; Ray, S.; Galvez, J.; Das, S. Fitness based weighted flower pollination algorithm with mutation strategies for image enhancement. *Multimed. Tools Appl.* **2022**, *81*, 28955–28986. [CrossRef]
35. Guha, R.; Alam, I.; Bera, S.K.; Kumar, N.; Sarkar, R. Enhancement of image contrast using selfish herd optimizer. *Multimed. Tools Appl.* **2021**, *81*, 637–657. [CrossRef]
36. Yan, Z.; Zhang, J.; Tang, J. Whale optimization algorithm based on lateral inhibition for image matching and vision-guided auv docking. *J. Intell. Fuzzy Syst.* **2021**, *40*, 4027–4038. [CrossRef]
37. Liu, J.J.; Shi, Q.H.; Zhao, J.; Lai, Z.H.; Li, L.L. Noisy low-illumination image enhancement based on parallel duffing oscillator and imogoa. *Math. Probl. Eng.* **2022**, *2022*, 3903453. [CrossRef]
38. Sun, Y.; Zhao, Z.; Jiang, D.; Tong, X.; Tao, B.; Jiang, G.; Kong, J.; Yun, J.; Liu, Y.; Liu, X.; et al. Low-illumination image enhancement algorithm based on improved multi-scale retinex and abc algorithm optimization. *Front. Bioeng. Biotechnol.* **2022**, *10*, 865820. [CrossRef] [PubMed]
39. Heidari, A.A.; Mirjalili, S.; Faris, H.; Aljarah, I.; Mafarja, M.; Chen, H. Harris hawk's optimization: Algorithm and applications. *Futur. Gener. Comput. Syst.* **2019**, *97*, 849–872. [CrossRef]
40. Dehkordi, A.A.; Sadiq, A.S.; Mirjalili, S.; Ghafoor, K.Z. Nonlinear-based chaotic harris hawks optimizer: Algorithm and internet of vehicles application. *Appl. Soft Comput. J.* **2021**, *109*, 107574. [CrossRef]
41. Zhang, B.; Lu, H.; Liu, S.; Yang, Y.; Sang, D. Aero-engine rotor assembly process optimization based on improved harris hawk algorithm. *Aerospace* **2022**, *10*, 28. [CrossRef]
42. Peña-Delgado, A.F.; Peraza-Vázquez, H.; Almazán-Covarrubias, J.H.; Torres Cruz, N.; García-Vite, P.M.; Morales-Cepeda, A.B.; Ramirez-Arredondo, J.M. A novel bio-inspired algorithm applied to selective harmonic elimination in a three-phase eleven-level inverter. *Math. Probl. Eng.* **2020**, *2020*, 8856040. [CrossRef]
43. Zhang, Y.J.; Yan, Y.X.; Zhao, J.; Gao, Z.M. Cscahho: Chaotic hybridization algorithm of the sine cosine with harris hawk optimization algorithms for solving global optimization problems. *PLoS ONE* **2022**, *17*, e0263387. [CrossRef] [PubMed]
44. Joshi, S.K. Levy flight incorporated hybrid learning model for gravitational search algorithm. *Knowl.-Based Syst.* **2023**, *265*, 110374. [CrossRef]
45. Gao, Y.; Zhang, H.; Duan, Y.; Zhang, H. A novel hybrid pso based on levy flight and wavelet mutation for global optimization. *PLoS ONE* **2023**, *18*, e0279572. [CrossRef] [PubMed]
46. Li, C.; Liu, J.; Zhu, J.; Zhang, W.; Bi, L. Mine image enhancement using adaptive bilateral gamma adjustment and double plateaus histogram equalization. *Multimed. Tools Appl.* **2022**, *81*, 12643–12660. [CrossRef]
47. Chen, J.; Yu, W.; Tian, J.; Chen, L.; Zhou, Z. Image contrast enhancement using an artificial bee colony algorithm. *Swarm Evol. Comput.* **2018**, *38*, 287–294. [CrossRef]
48. Xie, L.; Han, T.; Zhou, H.; Zhang, Z.R.; Han, B.; Tang, A. Tuna swarm optimization: A novel swarm-based metaheuristic algorithm for global optimization. *Comput. Intell. Neurosci.* **2021**, *2021*, 9210050. [CrossRef] [PubMed]
49. Xue, J.; Shen, B. A novel swarm intelligence optimization approach: Sparrow search algorithm. *Syst. Sci. Control Eng.* **2020**, *8*, 22–34. [CrossRef]
50. Peraza-Vázquez, H.; Peña-Delgado, A.; Ranjan, P.; Barde, C.; Choubey, A.; Morales-Cepeda, A.B. A bio-inspired method for mathematical optimization inspired by arachnida salticidade. *Mathematics* **2021**, *10*, 102. [CrossRef]
51. Arora, S.; Singh, S. Node localization in wireless sensor networks using butterfly optimization algorithm. *Arab. J. Sci. Eng.* **2017**, *42*, 3325–3335. [CrossRef]
52. Faramarzi, A.; Heidarinejad, M.; Mirjalili, S.; Gandomi, A.H. Marine predators' algorithm: A natureinspired metaheuristic. *Expert Syst. Appl.* **2020**, *152*, 113377. [CrossRef]
53. Mirjalili, S.; Lewis, A. The whale optimization algorithm. *Adv. Eng. Softw.* **2016**, *95*, 51–67. [CrossRef]
54. Takaoka, T.; Sato, M.; Otake, T.; Asaka, T. Novel routing method using slime mold algorithm corresponding to movement of content source in content-oriented networks. *J. Signal Process.* **2019**, *23*, 173–176. [CrossRef]
55. Mirjalili, S.; Gandomi, A.H.; Mirjalili, S.Z.; Saremi, S.; Faris, H.; Mirjalili, S.M. Salp swarm algorithm: A bio-inspired optimizer for engineering design problems. *Adv. Eng. Softw.* **2017**, *114*, 163–191. [CrossRef]